ZEPHYR

Towards a more efficient exploitation of on-shore and urban wind energy resources

Research and Innovation Action
Call: H2020-ITN-2019-1
Call topic: MSCA-ITN-2019 - Innovative Training Networks
Project start: 1 November 2019 Project duration: 48 months

D5.10: Application to existing and new benchmarks: WP5 Final Public Report (T5)

Executive summary
This report presents the different methodologies used by several ESRs to predict the aerodynamic and aeroacoustic performance of a horizontal axis wind turbine. The case study is an SWT-2.3-93 wind turbine located at the Høvsøre Wind Turbine Test Center in Denmark. Information about the atmospheric conditions and wind turbine noise is available in the literature. Furthermore, the CAD of the wind turbine is reconstructed with the available information. The database is published openly in a Zenodo database. As intermediate validation, analyses on a 2D symmetric airfoil, representative of the wind turbine's outer rotor, were conducted and compared with wind tunnel results conducted by the ESRs. The main results consisted of atmospheric boundary layer simulations, wind turbine aerodynamic performance, far-field noise prediction, and auralization noise.

Partner in charge: SGRE

Project co-funded by the European Commission within Horizon 2020 Dissemination Level		
PU	Public	PU
PP	Restricted to other programme participants (including the Commission Services)	–
RE	Restricted to a group specified by the Consortium (including the Commission Services)	–
CO	Confidential, only for members of the Consortium (including the Commission Services)	–

This project has received funding from the European Union's Horizon 2020 research and innovation programme under grant agreement No 860101

Deliverable Information

Document administrative information	
Project acronym:	**ZEPHYR**
Project number:	**860101**
Deliverable number:	**5.10**
Deliverable full title:	**Application to existing and new benchmarks: WP5 Final Public Report**
Deliverable short title:	**WP5 final report**
Document identifier:	**ZEPHYR-510-WP5 final report-T5-Final-v1.0**
Lead partner short name:	**SGRE**
Report version:	**v1.0**
Report submission date:	**18/09/2023**
Dissemination level:	**PU**
Nature:	**Report**
Lead author(s):	**Laura Botero-Bolivar (UTW)**
Co-author(s):	**Baris Kale (VKI), Kartik Venkatraman (VKI), and Shubbam Shubbam (NTU)**
Status:	**Final**

The ZEPHYR Consortium partner responsible for this deliverable has addressed all comments received. Changes to this document are detailed in the change log table below.

Change log

Date	Version number	Author/Editor	Summary of changes made

Table of Contents

List of abbreviations

AL	Actuator line
BEMT	Blade Element Momentum Theory
CAD	Computer Aided Design
CFD	Computational Fluid Dynamics
DoA	Description of Action
EC	European Commission
ECMWF	European Centre for Medium-Range Weather Forecasts
FSI	Fluid Structure Interaction
GFS	Global Forecast System
LES	Large Eddy Simulation
LE	Leading edge
NACA	National Advisory Committee for Aeronautics
OC	Operational condition
RANS	Raynolds Average Navier Stokes
TSR	Tip Speed Ratio
TE	Trailing edge
WRF	Weather Research and Forecasting

List of Figures

1 Introduction and objectives

The project zEPHYR aims to analyze the effect of installing wind turbines in complex terrains and urban areas. The project focuses on human factors and societal acceptance as well as on the improvement of the prediction models for aerodynamic performance, structural dynamics, and noise production. To do so, three benchmarks were defined to cover the essential topics the project aims to address. They are:

- T5.1: Horizontal axis wind turbine: this benchmark aims to define a horizontal axis wind turbine as a case of study where the ESRs could apply their different methodologies to the same case, which would allow to compare the results among the ESRs and measurements of the actual wind turbine and environment.
- T5.2: Complex terrain: in this benchmark, the objective was to conduct simulations of meso and microscale, which allows the characterization of complex terrain and incorporates the effect of such complex terrain on wind turbine noise production and propagation.
- T5.2: Urban canopy: this benchmark consists of analyzing the flow around buildings and how the wind energy can be hastened with vertical axis wind turbines.

In this public report, the main objectives and results achieved by each of the benchmarks are presented.

2 T5.1: Large Horizontal Axis Wind Turbine

The large on-shore horizontal axis wind turbine benchmark is based on acoustic measurements (Leloudas, 2006) made on a SWT-2.3-93 wind turbine on the Høvsøre Wind Turbine Test Center in Denmark, for which the met mast data are also available for the corresponding time period. Even if the geometry and the operating curves are not available, good approximate models for the STW-2.3-93 WT are available in the literature, as detailed below. The available data allow then performing of a complete simulation chain validation, from weather re-forecast to noise predictions.

The SWT-2.3-93 wind turbine is a variable-speed variable-pitch turbine, and to determine a specific operational condition, it is necessary to identify a rotor speed and a blade pitch angle. For above-rated operations, the blade pitch angle is changed with respect to the reference below-rated value to keep the nominal power output constant for increasing wind speed. The below-rated pitch angle setting is an important parameter for a wind turbine, as it refers to the optimal angle of attack at the blade cross-sections. However, in the Churchfield report (Churchfield, 2013), the below-rated pitch angle setting was not clearly indicated, and a short sensitivity study was conducted to find a suitable value maximizing the power output.

At below-rated conditions, the wind turbine operates at constant TSR, and the power curve (Power P vs wind speed U) follows the ideal $P \approx U^3$ law. As already discussed, in the Churchfield report (Churchfield, 2013), the blade properties were guessed by trying to match the manufacturer's power curve, which assumes a design TSR=6, see Fig.1-(a). However, Churchfield could achieve the best match for TSR=8.4, as shown in Fig.1-(b). Given this ambiguity, the sensitivity analysis considered three TSR values, namely 6.0, 7.2, and 8.4, and for each of them, a range of blade pitch settings was simulated from -5.0 to 5.0deg. For this analysis, the turbine was simulated by the Samcef BEMT code as an isolated rotor with rigid blades, no tilt angle, and for a uniform, steady axial wind inflow of 9.25 m/s in order to cancel all possible sources of unsteadiness and reach a steady state power output. Finally, the chord, twist, and airfoil polars provided in the Churchfield report were used as input parameters for the simulations.

The results of this sensitivity study are shown in Fig.2, where the below-rated power output for the TSR values studied is plotted against the blade pitch setting. We can see that for all three TSR values, the power output is maximized for a specific blade pitch setting. Moreover, as suggested by Churchfield

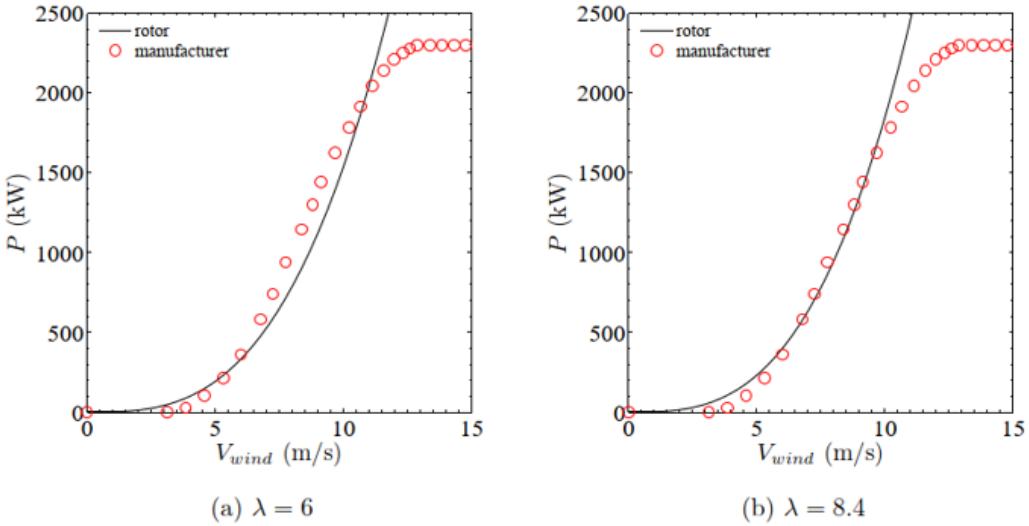

Figure 1: Effect of the TSR on the power curve for the Siemens SWT-2.3-93 wind turbine according to (Churchfield, 2013).

(Churchfield, 2013), the power output for the optimal pitch setting increases for increasing TSR and is indeed the largest for TSR=8.4. In any case, The optimal blade pitch setting is in the neighborhood of 0deg for all TSR curves with 1deg variation. From an aerodynamic point of view, it could be argued that 1deg uncertainty in the AoA estimation might lead to some variation in the aerodynamic load estimation, while for aeroacoustics purposes, it might have a small, if not negligible, effect.

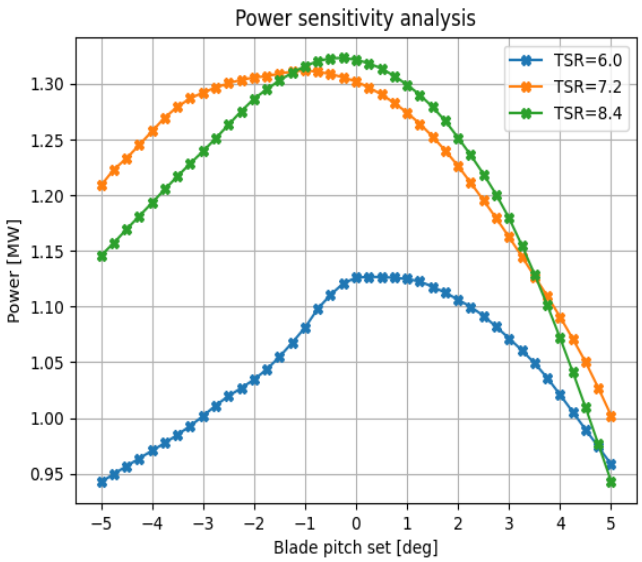

Figure 2: Results of the sensitivity analysis to find the suitable below-rated blade pitch setting for the Siemens SWT-2.3-93 wind turbine.

2.1 Location and time stamp

The Høvsøre Wind Turbine Test Center is located in the northwest of Denmark. The test center is located on a flat terrain and includes five wind turbines and six meteorological masts spaced about three hundred meters apart. During the acoustic experiments, only the SWT-2.3-93 WT, located at position WT5 in Fig. 3b, is operating while the other wind turbines are stopped.

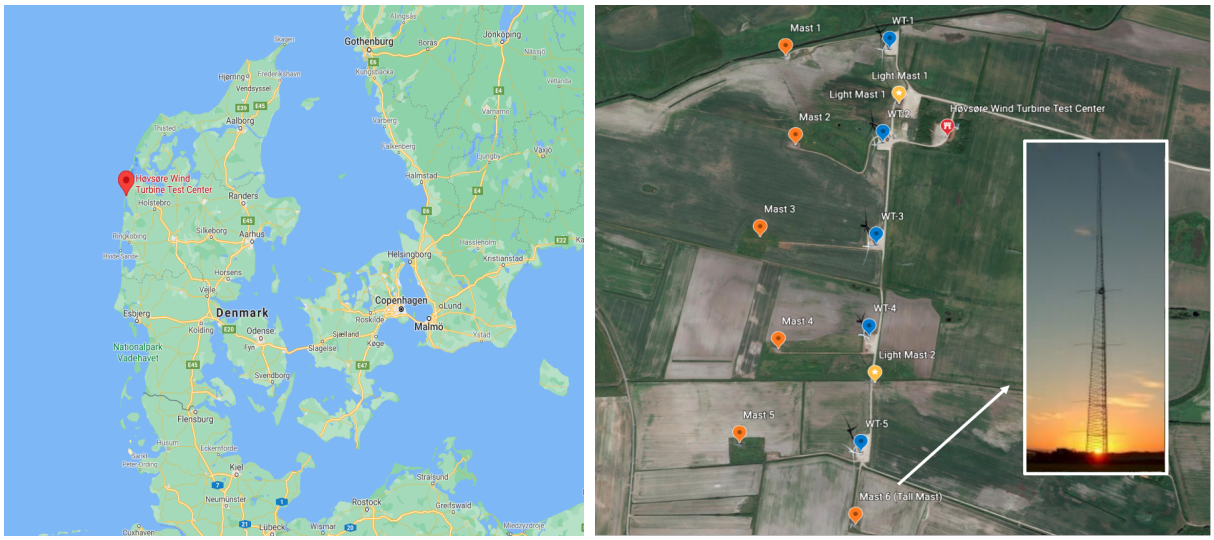

(a) Location of the Høvsøre Wind Turbine Test Center. **(b)** Locations of the wind turbines and meteorological masts.

Figure 3: Høvsøre Wind Turbine Test Center in Denmark.

Meteorological data are available via online plots at the website of the Technical University of Denmark Wind Energy Department (DTU, 2021). The weather data such as wind speed, wind direction, temperature, radiation, pressure, and humidity are measured at Mast 6 (Tall Mast), which is an intensively equipped 116.5 m tall mast located at the coordinates 56.441 (latitude) and 8.151 (longitude) as shown in Fig. 3b. Data collected from sonic anemometers are logged at 20 Hz, cup anemometers and wind vanes at 10 Hz, and climatological parameters such as temperature, pressure, and humidity at 1 Hz. The available data are sampled and averaged in periods of 10 minutes.

Acoustic measurements obtained during 2-days of tests performed under design and off-design operating conditions in 2006 are available in the master's thesis project of Giorgos Leloudas (Leloudas, 2006) in terms of noise spectra.

2.2 Wind turbine geometry and operating conditions

The SWT-2.3-93 is a 2.3 MW (rated power) horizontal axis wind turbine with a rotor diameter of 93 m built by Siemens Gamesa (Fig. 4a). The rotor speed ranges from 6 to 16 RPM, and the hub height is 80 m. The cut-in and cut-out speeds are, respectively, 3 and 25 m/s (Leloudas, 2006).

An approximated geometry was reconstructed by Churchfield (Churchfield, 2013) based on a reverse engineering method. The Generic Siemens SWT-2.3-93 is composed by FFA and NACA (63 family) airfoils of variable chord and twist angle obtained from National Renewable Energy Laboratory's (NREL) *WT_Perf* code (Buhl, 2011). The normalized chord, twist, and thickness distributions along the span were first denormalized following the steps in Leloudas' report (Leloudas, 2006); then pitch & torque control systems were introduced to optimize and closely match the manufacturer's power curve using the blade element momentum theory (see Fig. 5).

(a) SWT-2.3-93 wind turbine, Windtest Grevenbroich, Germany.

(b) SWT-2.3-93 wind turbine used in acoustic test at Høvsøre Wind Turbine Test Center.

Figure 4: Siemens 2.3 MW 93 meter rotor diameter wind turbine.

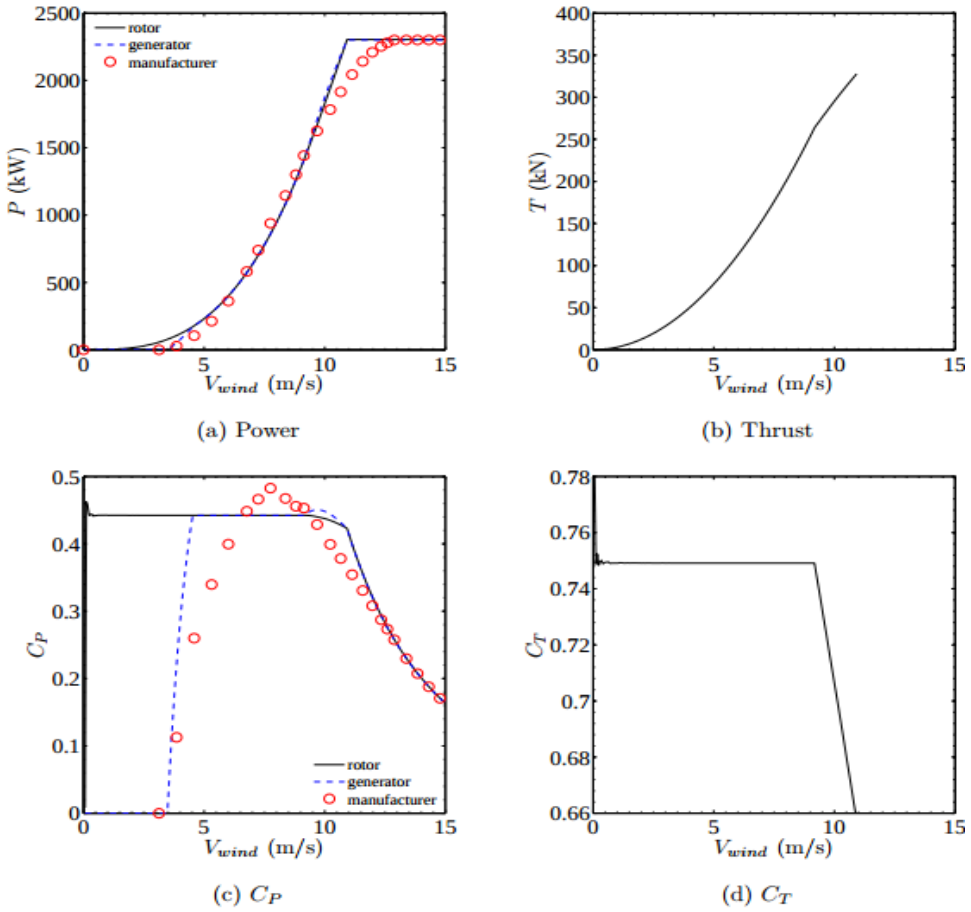

Figure 5: Power and thrust data with non-dimensional coefficients for the Generic Siemens SWT-2.3-93 wind turbine (Churchfield, 2013).

The three operating conditions (OC) used in this benchmark are chosen to match the acoustic measurements of (Leloudas, 2006). They are summarized in table 1, and they will be referred to in the following

Table 1: Operating Conditions (OC) simulated.

	OC1	OC2	OC3
Rotor speed [rpm]	13	14	17
Pitch angle [°]	3	-2	5
Wind speed at 80 m [m/s]	6	8	9.5

as OC1, OC2, and OC3. These conditions are *off-design* conditions, meaning that the pitch angle is not the one prescribed by the controller to obtain the optimal power output, but it was changed to investigate the effect of the pitch angle on the noise emissions.

The information collected about the wind turbine is published in an open database in Zenodo in *https://zenodo.org/record/73* referred to as (Christophe & Oerlemans, 2022).

2.3 Methodologies and interaction among the ESRs

Table 3 shows the ESRs that are participating in this case of study together with their host institution.

Table 2: Participation of the ESRs.

ESR	Name	Institution
1	Baris Kale	VKI
3	Laura Botero	UTW
6	Nishchay Tiwari	IMP-PAN
8	Andrea Bresciani	SISW
9	Umberto Boatto	Samtech
12	Oscar Mariño	UPM

The flowchart describing the methodologies, ESRs involved, and required input/outputs for each phase of the benchmark activities is shown in Fig.6. This diagram cleary shows the interaction among the work of the ESRs. This benchmark addresses three different physics domains corresponding to three specific types of analyses. First, the modeling of the turbulent atmospheric wind by WRF-LES will be carried out by ESR 1. Second, the aerodynamic modeling of the turbine rotor by BEMT and CFD will be done by ESR 1, 9, and 12. Third, ESRs 1, 3, and 8 will perform LE and TE noise modeling by using different methods. Finally, as part of the noise predictions, ESR 8 will also conduct noise auralization studies.

The three domains will be investigated sequentially by exploiting the outputs of the previous domain analyses as well as input data and conditions. The WRF-LES performed by ESR 1 take inputs from the met mast data and turbine location and provide the turbulent field for the aerodynamic and aeroacoustics analyses. The ESRs involved in the aerodynamic analysis also require the wind turbine CAD geometry and parameters for their simulations and provide rotor aerodynamic data for the noise modeling. Within the noise block, a preliminary step provides the boundary layer characteristics from the rotor aerodynamic data to the various LE and TE models, which will be calculated for a single airfoil and compared with wind tunnel measurements conducted by ESR 3. The acoustic outputs of the far-field noise will be used for noise auralization to get the audible signal.

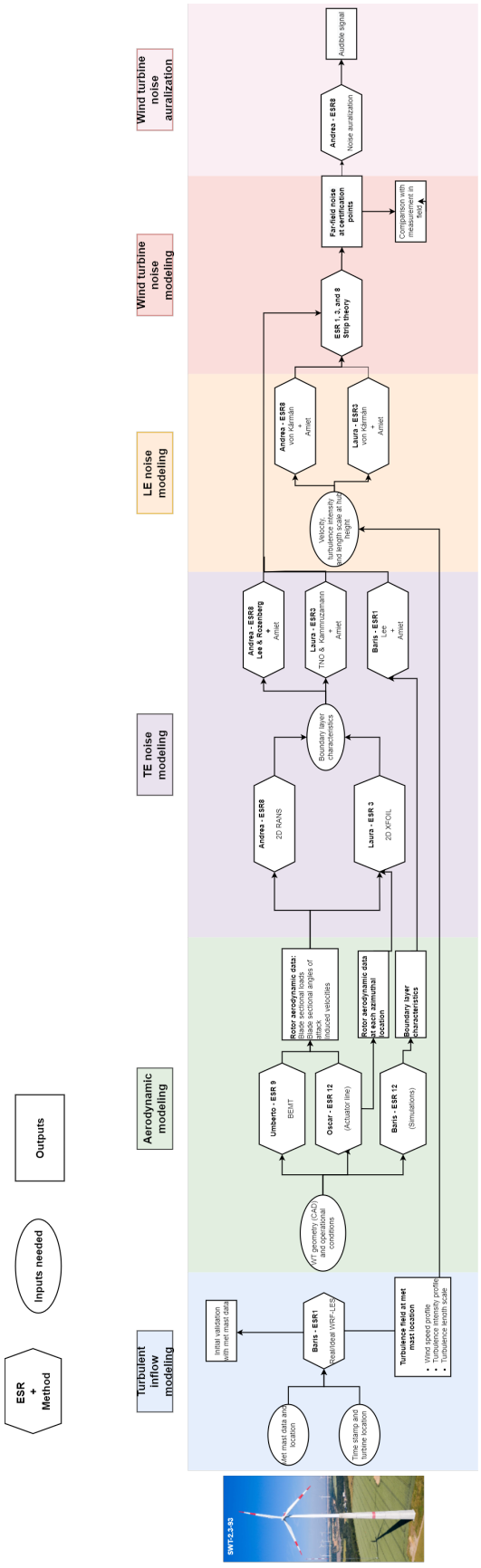

Figure 6: Distribution of tasks for each ESR for large horizontal axis wind turbine case study.

2.4 Results

2.4.1 Atmospheric simulations:

Figure 7 shows vertical profiles of time-averaged horizontal wind speed, $\overline{U}$, wind direction, $\overline{\beta}$, and temperature, $\overline{T}$, as well as turbulence intensity, TI, from numerical results corresponding to WRF-LES-d05, and experimental data from the Høvsøre mast. WRF-LES results were obtained from the time series of 200 Hz data, whereas experimental data were obtained by averaging the 10-min averages over the period of interest. The undisturbed wind speed profiles overestimate the measured data; however, the wind speed profile obtained in the wake of the wind turbine matches the mean values of the experimental data above 60 m, demonstrating the influence of the wake on the wind speed measurements at the met mast location. In addition, the backward S-shaped profile in the measured wind speed indicates a deceleration of the wind speed along the wind turbine rotor during the measurement campaign. When backing winds occur, the backward S-shaped wind speed and wind direction profiles can be observed. Nonetheless, the wind direction profile was nearly flat, and no backing wind occurred during the relevant measurement period, proving the wake effects on the measured weather data. The reason why the wind direction profile in the wake of the wind turbine differs from the experimental data is probably due to the selection of the control point location. The temperature profiles show a trend commonly observed in typical unstable ABL conditions because the temperature drops with altitude as the earth is heated by the sun. Higher turbulence levels were observed in the wake of the wind turbine due to enhanced turbulence mixing caused by the wake rotation. Here, TI was calculated from the three velocity components and normalized by the mean wind speed at hub height. The reader is referred to 8 for the layout of the WRF-LES control points.

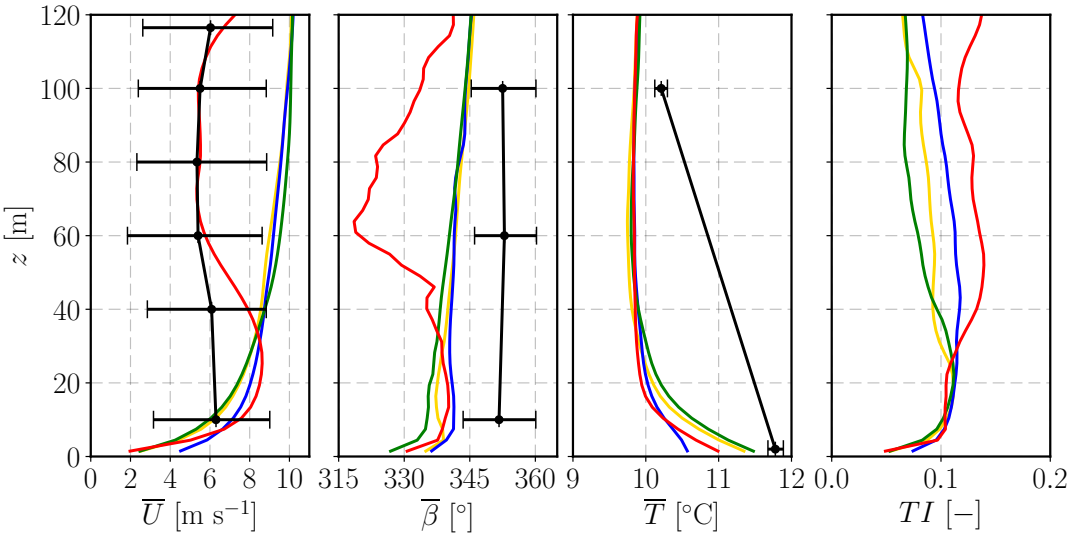

Figure 7: Vertical profiles of time-averaged horizontal wind speed, $\overline{U}$, wind direction, $\overline{\beta}$, and temperature, $\overline{T}$, as well as turbulence intensity, TI, from numerical results corresponding to WRF-LES-d05, and experimental data from the Høvsøre mast. Solid black lines with horizontal bars correspond to experimental data with minimum and maximum values. A solid blue line denotes the WRF-LES results at the met mast location, a solid yellow line denotes the results at a control point upstream of the wind turbine in the northwest direction (CP-inflow1), solid purple line stands for the results at a point one rotor diameter upstream of the wind turbine (CP-inflow2), solid green line denotes the results at a control point upstream of the wind turbine in the northeast direction (CP-inflow3), and solid red line denotes the model predictions at a control point in the wake of the wind turbine close to the met mast (CP-wake).

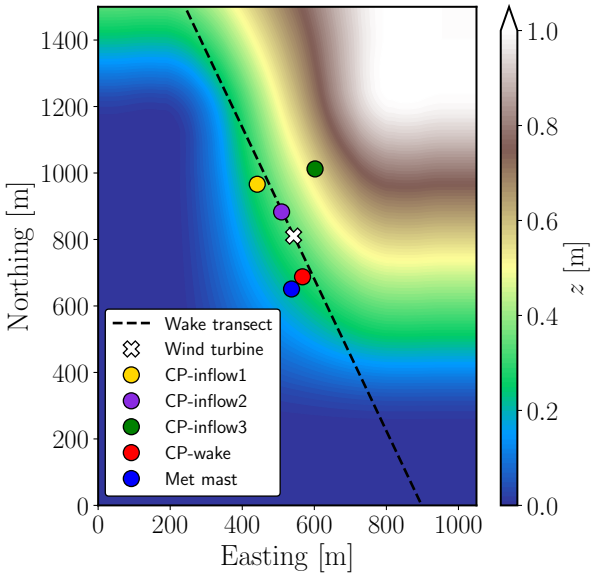

Figure 8: Illustration of the finest-resolution WRF-LES domain (WRF-LES-d05) colored by terrain height. The dashed line denotes the wake transect, whereas the solid white cross depicts the location of the SWT-2.3-93 WT. Filled circles show the locations of the control points and the Høvsøre mast. CP stands for the control point.

2.4.2 Aerodynamic results:

Figure 9 shows the comparison of the blade loading obtained with actuator line simulations and blade element momentum theory methodologies for the operational condition 2. The results show a good agreement among both methodologies. The same kind of results are obtained for the other methodologies, not shown here for the sake of simplicity.

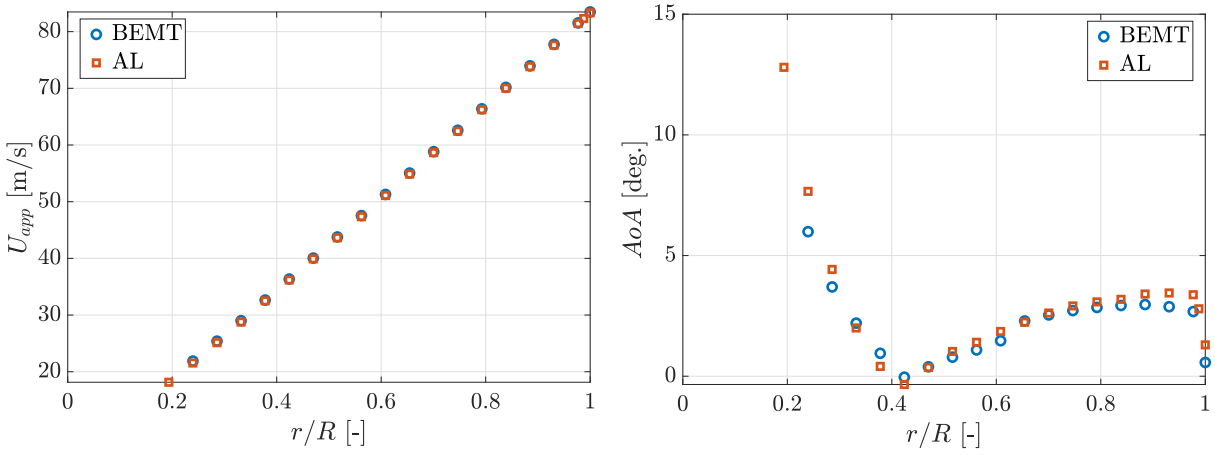

(a) Apparent velocity

(b) Angle of attack

Figure 9: Comparison of the blade loading obtained with BEMT and AL for OC 2.

In addition, instantaneous results of the local variables along the whole blade are stored as will be used in the noise prediction shown in section 2.4.3. The local velocity and angle of attack can be seen in Fig. 10 for several locations along the blade for one revolution of the turbine. In addition, it is compared with the average values.

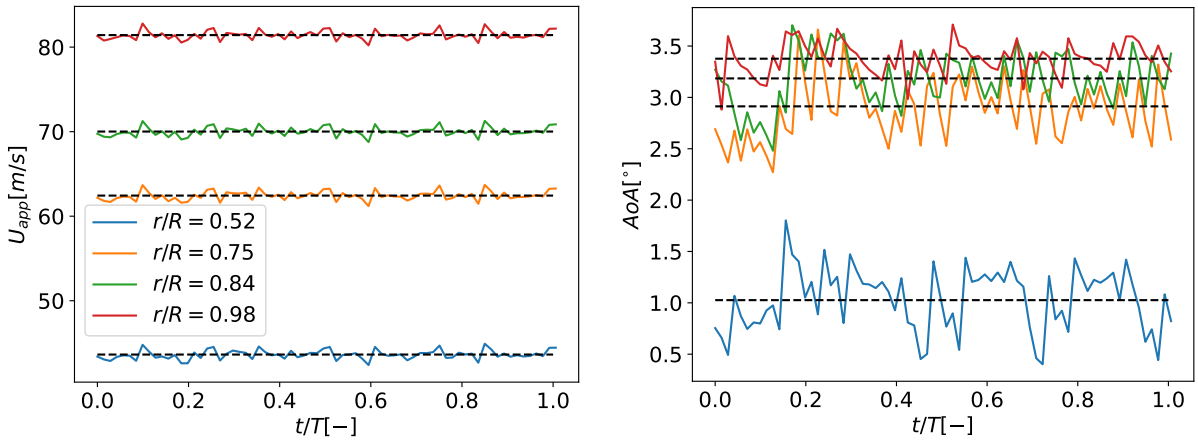

(a) Apparent velocity

(b) Angle of attack

Figure 10: Evolution of the local variables at certain locations on the blade in one revolution for the AL results. Average results are shown in black dashed lines.

2.4.3 Acoustic results:

In this section, the noise predicted with the several methodologies used by the ESRs is presented for the three operational conditions compared with the experimental measurements in Figure 11. The figure also includes the lines for the uncertainty of the measurements.

For the OCs 1 and 3, there are no large differences in the low-frequency range for the different methodologies. The large difference in the high-frequency range between the far-field noise prediction and the Harmonoise propagation model is because of the atmospheric absorption that is neglected in the far-field noise prediction, as explained before. For the OC2, the differences among the methodologies are larger, most probably because of the separation detected by XFOIL and in the GAL + RANS methodology that was not detected by the steady RANS simulations. The poo agreement in the low-frequency range for the “LES + GAL + RANS” methodology compared with the others is because this approach does not consider the leading-edge noise, which is responsible for the low-frequency noise, as shown in Figure **??**.

In OC 3, it is evidenced that considering the instantaneous or averaged results of the AL simulations, the wind turbine noise is not affected. This is because there is no source of change in the blade loading over one rotation. The different noise intensity observed at each azimuth location is due to the change of the noise directivity at each position with respect to a fixed observer. This might differ if a source of non-axisymmetric is incorporated into the AL simulations, e.g., a tower or the wake of an upstream wind turbine. However, this study remains a proposal for future work.

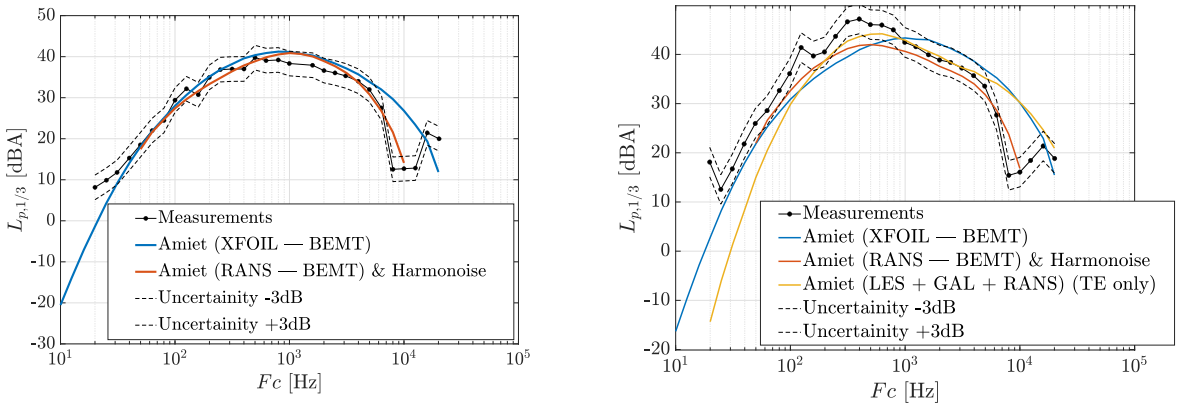

(a) OC1

(b) OC2

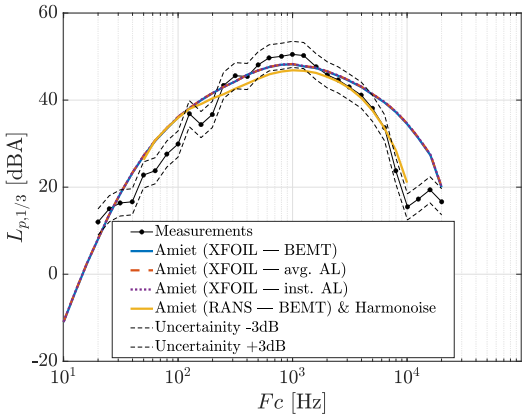

(c) OC3

Figure 11: Far-field noise for the several operational conditions obtained with the different methodologies.

3 T5.2: Complex terrain

The scarcity of flat terrain availability for wind-farm development has shifted the focus towards the utilization of complex terrains, which constitute 70% of the Earth's surface. This potential for wind energy harvesting, as well as the advantage of remoteness from urban communities, which reduces the nuisance due to wind turbine noise, is significant. However, complex terrains remain very challenging areas to consider for wind farm siting due to the following considerations:

- Wind farm modeling requires a more advanced approach than commonly used cost-effective linearized models, which cannot handle complex phenomena (i.e., flow separation)
- Wind resource assessment requires to account for the multitude of different temporal and spatial scales.
- Wind turbine noise propagation can be strongly affected by topography and the complex flow field. While wind turbines are often placed along ridges to benefit from the wind speed-up, noise issues may still remain a key environmental factor even in such areas that are usually found further away from urban communities.

To address the above challenges, a benchmark case was chosen to develop numerical models and address existing research gaps. The complex terrain site of Perdigão was chosen for benchmarking due to the availability of a wide range of field measurement data as listed on the Perdigão website (*Perdigao Field Experiment*, 2017). An extensive field measurement campaign was carried out at the Double Ridge site in Perdigao, Portugal, by a joint US/European program partially funded by the EU. The campaign spanned a period of 183 days (26 weeks) from December 15, 2016, to June 15, 2017. The site is located at San Gregorio near the Centre of Portugal, comprising two parallel ridges with northwest orientations, separated by 1.5 km, 4 km long, and 500, 550 m tall at their summit. The site is covered by a short heterogeneous canopy over the entire terrain. An elevation map of the terrain is shown in Fig. 12.

Table 3 shows the different participants of this benchmark and the project objectives. The topic and exchange of information for this benchmark is illustrated in the flowchart shown in Fig 13, highlighting the different simulation approaches and methodologies.

Table 3: Participation to the benchmarks.

ESR#	Name	Institution	Title of contribution
-	NAME	INSTITUTION	Eg. Perdigao Mesoscale, Microscale, Noise, Turbine etc
1	Baris	VKI/UPM	Meso(PBL)-micro(LES) coupled wind turbine simulations using WRF
2	Kartik	VKI/UdeS	Microscale simulation modelling with different source terms
3	Laura	UTW	Wind turbine noise generation
8	Andrea	SISW/CSTB	Wind turbine noise propagation
9	Umberto	SAMTECH-SISW	Wind turbine aero-elasticity
13	Mohanad	UPM	synthetic realization (time/space series)

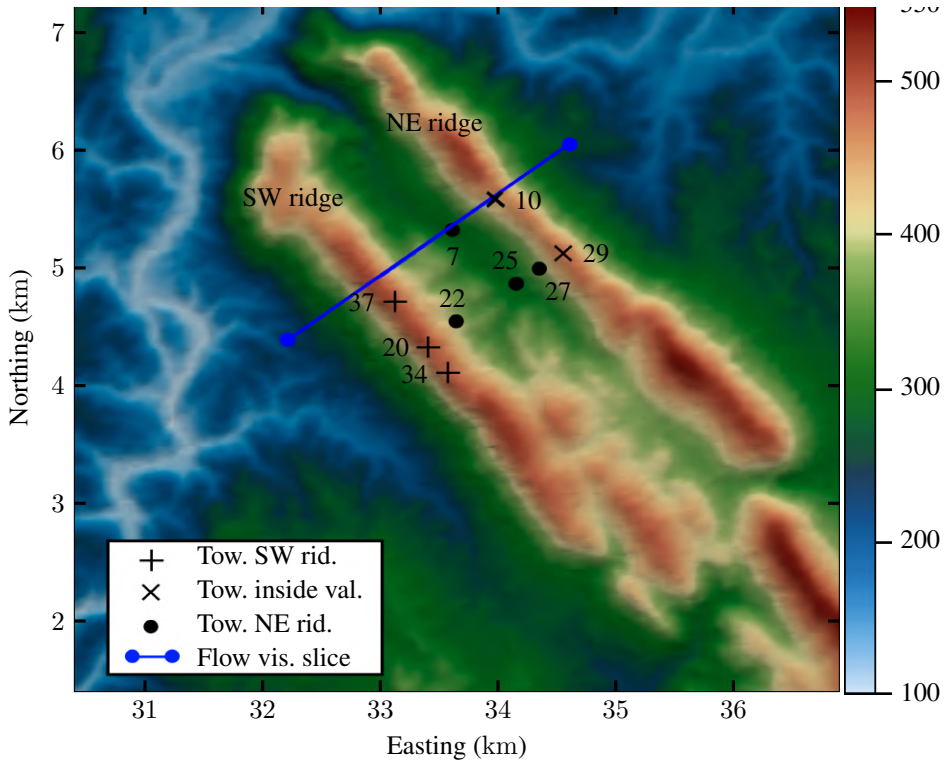

Figure 12: Elevation map and locations of interest at Perdigao. Positions of the measurement towers in the SW ridge group are indicated with + symbols; likewise, NE masts are marked with an x, and the masts in the inside valley group are indicated with black dots. PT-TM06/ETRS89 coordinate system, height above sea level.

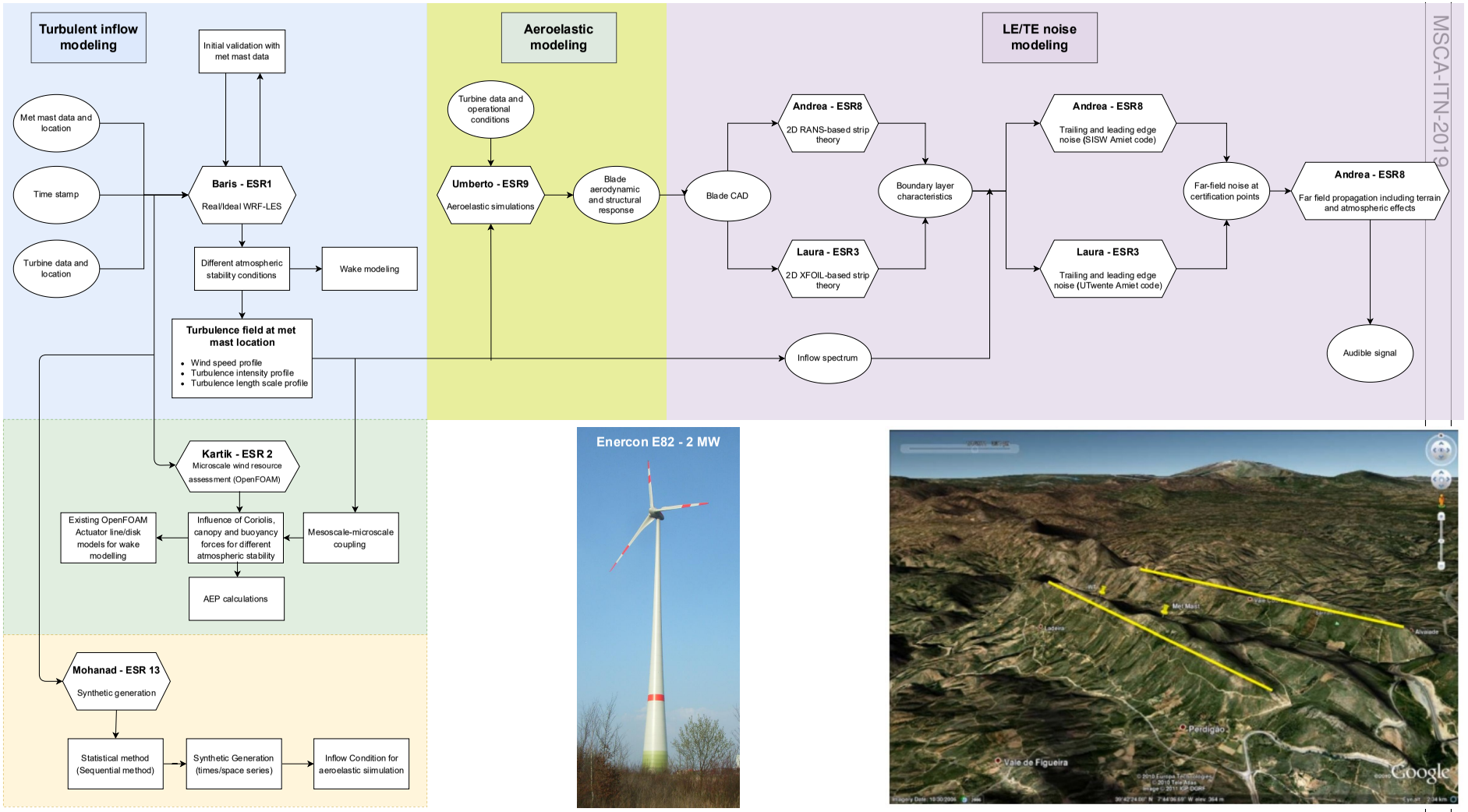

Figure 13: Flow charts showing different research topics and exchange of information among different ESRs, also shown is an image of the Enercon E82 turbine and the Perdigao double ridge (*Perdigao Field Experiment*, 2017).

3.1 Key Findings

3.1.1 Atmospheric Flow simulations

Micro-scale simulations using OpenFOAM showed that the inflow direction and model source terms in microscale simulations play an important role in atmospheric flow prediction over complex terrain (Venkatraman, Hågbo, Buckingham, & Giljarhus, 2023). For example, the impact of inflow direction is shown in Fig. 14.

The WRF-LES models show that they can reproduce three-dimensional microscale flow structures observed on top of the ridges and in the valley of the Perdigão site. The domain used for the model is shown in Fig. 15. The simulated turbulent flow field results have been compared with existing experimental data from the Perdigão experimental campaign. Numerical results from the met masts have shown that the time series and vertical profiles of horizontal wind speed, wind direction, and potential temperature agree reasonably well with experimental data despite minor differences in the vertical profiles of horizontal wind speed over the ridges and wind direction in the valley. For all the atmospheric stability cases tested, the WRF-LES model overestimates the 1-hour average horizontal wind speed at hub height on the order of 1-5 $\mathrm{m\,s^{-1}}$ over the ridges (TSE04 and TSE13) and in the valley (TSE09).

3.1.2 Wind turbine simulations

Low-fidelity aerodynamic simulations of the Vestas -V80 turbine were performed by means of the Blade Element Momentum Theory (BEMT) approach for the neutral and unstable atmospheric stability conditions. WRF-LES wind flow components can be used to provide suitable input for BEMT simulations. Specifically, in the case of significant wind shear due to unstable atmospheric conditions, careful attention should be paid to the scaling of the geo-potential height of the probing locations with respect to the ground location at such a site and at the turbine location. Furthermore, the wind direction in proximity of the turbine must be considered to be able to select the most appropriate upstream location for the probing of the WRF-LES wind. This study represents only a first step in this direction, and further analysis is recommended.

3.1.3 Acoustic Simulations

Acoustic measurements from DLR are compared to numerical predictions in the complex terrain of Perdigão accounting for atmospheric conditions using the Harmonoise meteorological model. The LES results from B. Kale are used to obtain an estimate of the site-specific turbulence intensity and integral length scale to model the leading-edge noise. The BEMT results from U. Boatto are used to obtain the induced angles of attack and apparent inflow velocities for the RANS simulations of the blade sections. With regards to noise propagation, the study demonstrated the feasibility of applying the numerical method developed for complex terrains and atmospheric conditions. The generated noise maps such as shown in Fig. 16 show the effect that ground topology under different stability conditions. That is, the larger radius of curvature of the ray paths caused by the smaller sound speed gradient increases the screening effect of the ground topology.

Further details on the different model setups and results can be found in the zEPHYR deliverable "D5.5: Complex Terrain Benchmark Final Report" and published literature.

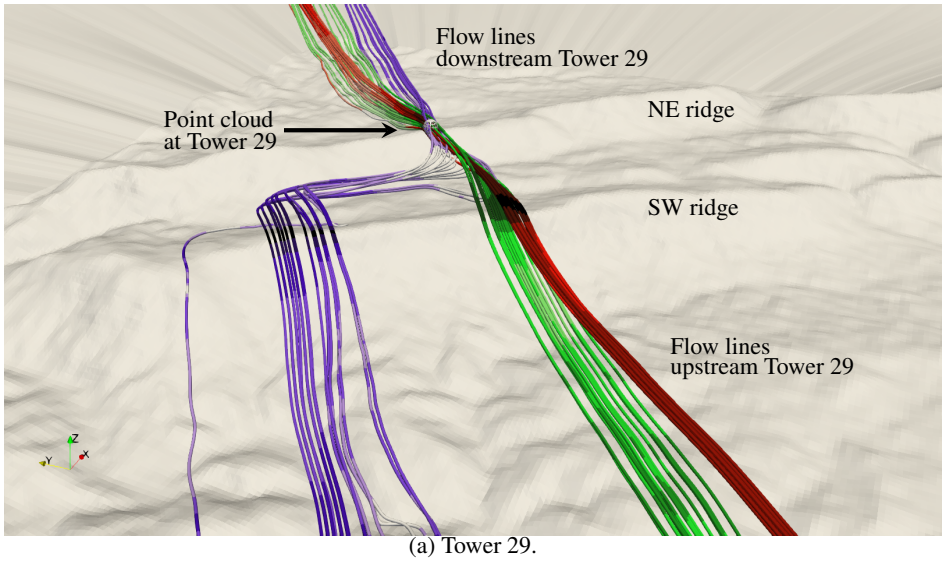

(a) Tower 29.

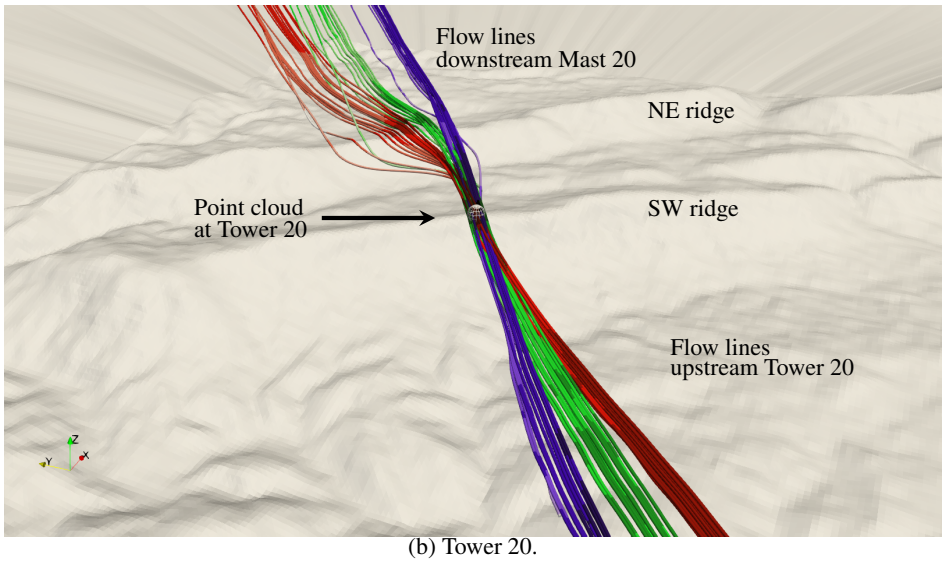

(b) Tower 20.

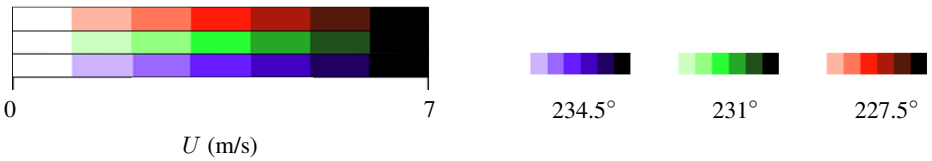

Figure 14: Wind paths of air parcels passing through a sphere of 55 m radius placed on top of the ground at given met mast locations. Flow lines colored in green represent trajectories for wind coming from 231° at the inlet, while red and blue lines illustrate wind at the inlet from 227.5° and 234.5° correspondingly.

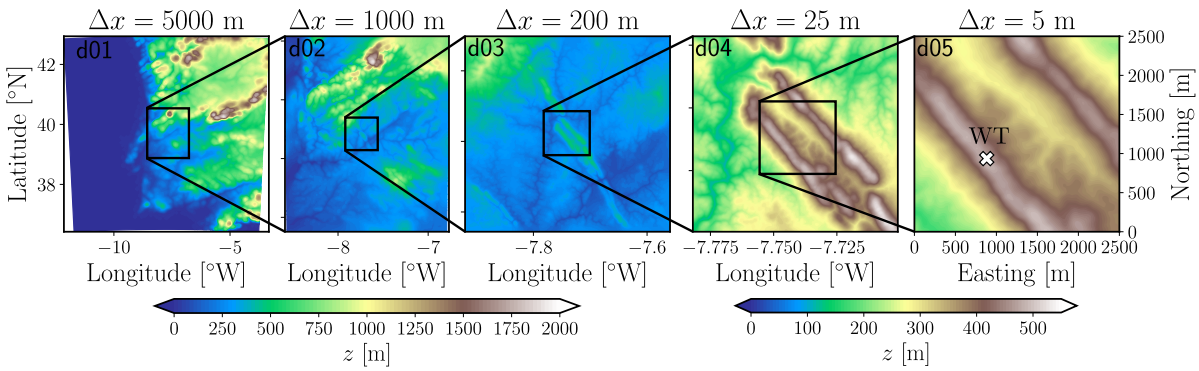

Figure 15: Nested domain configuration from the multi-scale WRF-LES simulation. All nested domains centered on the Perdigão site are colored by terrain height where $z = 0$ m corresponds to sea level. The five domains have resolutions of 5000 m, 1000 m, 200 m, 25 m, and 5 m.

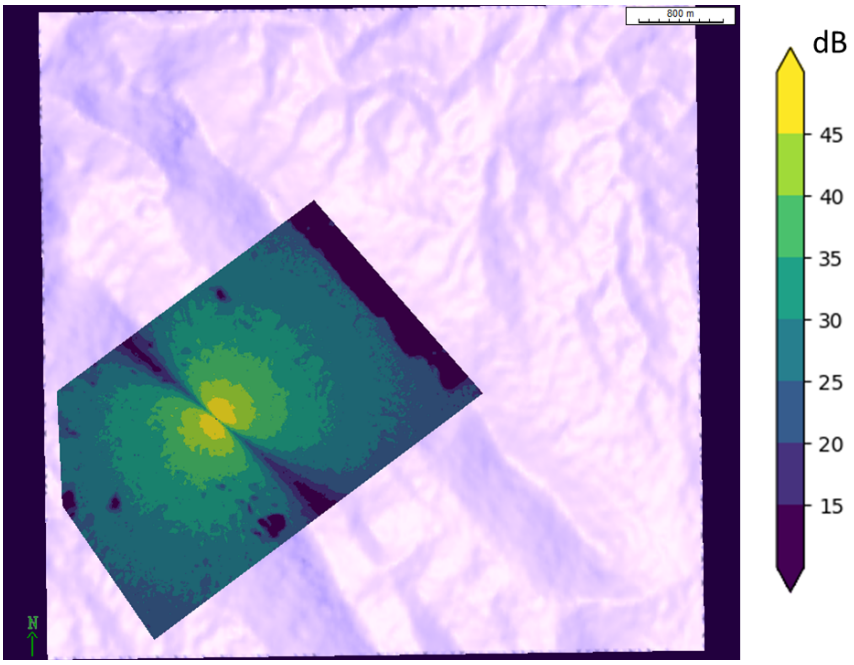

(a) Neutral atmosphere

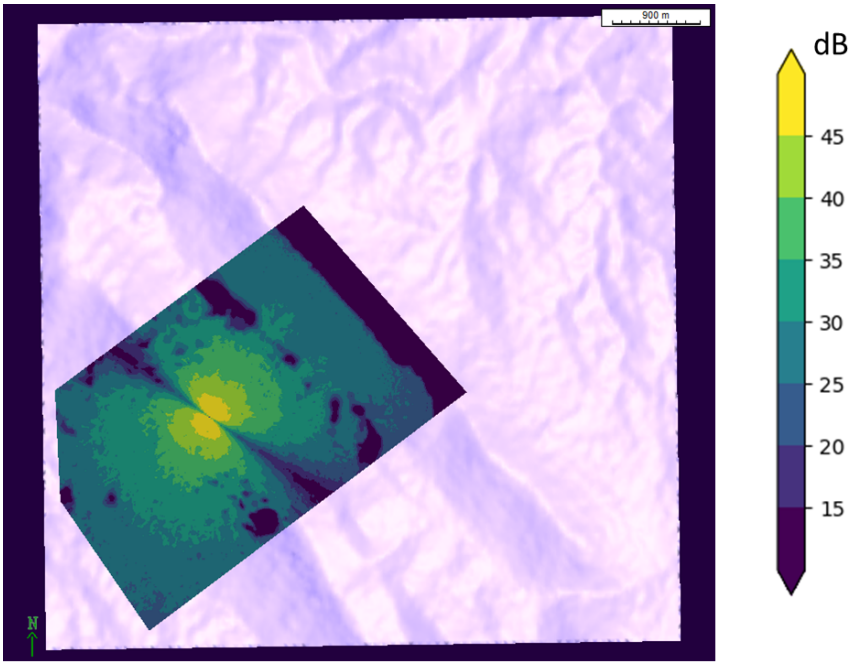

(b) Unstable atmosphere

Figure 16: Predicted, overall noise levels between 63 Hz and and 8 kHz, 1.5 m above the ground.

4 T5.3: Urban canopy

4.1 Definition

Defined as the distance from the ground to the roof of buildings, the urban canopy layer (UCL) is a significant aspect of urban architecture (Micallef & van Bussel, 2018), whereas the urban boundary layer (UBL) encompasses the region extending from the roof of buildings and beyond, marked by the influence of the urban canopy as depicted in Fig 17; the intrinsic quality of the urban micro-climate plays a pivotal role in driving the performance of wind turbines situated within urban confines, leading to comprehensive urban wind resource assessment studies designed to pinpoint the optimal locations for the installation of wind turbines, with a marked preference for regions demonstrating high flow acceleration such as building rooftops, and a conscious avoidance of areas characterized by high turbulence intensity and re-circulation zones.

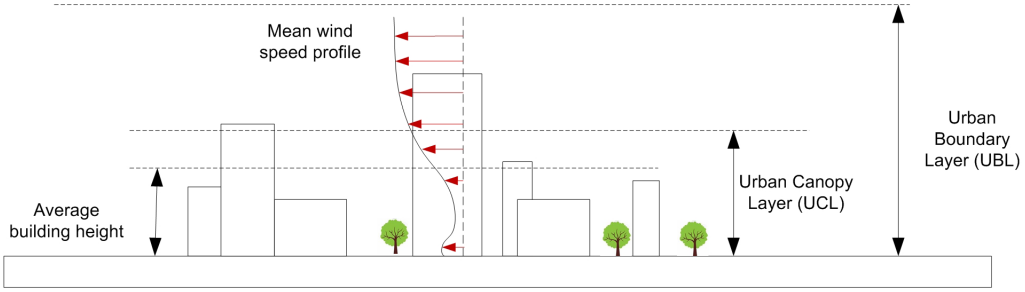

Figure 17: Urban wind profile depicting the urban canopy layer and the Urban boundary layer (Ng et al., 2011)

Wind Resource assessment

(Ng et al., 2011)Wind measurements in urban areas are usually performed using instrumentation placed close to buildings. However, in most places, local instrument data is not available, which necessitates the need for CFD models. Several methods exist for urban wind resource assessment, such as:

- Local field instrumentation such as a cup or sonic anemometers and extrapolation to different heights using log-law assuming a neutral atmospheric boundary layer profile.
- Scaling using wind tunnel models and measurements
- Using wind speed probability distribution functions from surrounding available areas/ weather stations.
- Correction factors using wind resource maps developed from regional wind atlas.

Flow around buildings

Flows in the urban environment, which encompasses flow around various urban elements such as buildings and trees, present complex features like regions of flow acceleration, corner streams around building edges, separation bubbles over rooftops, and wake deficits on the leeward side, all vividly depicted in Fig 18; furthermore, the specific shape of building roofs emerges as a key factor in locally altering wind resources, with the phenomenon of flow acceleration over sloped rooftops representing a potentially favorable characteristic that can be strategically harnessed to augment wind resource yields.

Forest canopy

Forested areas around cities can play a critical role in the urban wind conditions. A percentage of 183 million hectares of forest, which covers 43 % of the EU's land (Negre, 2020), requires the illumination of potential wind farm sites also in forested regions (Meier, 2012). Forests have a strong influence on wind conditions by decreasing the wind speed and creating turbulence. Aiming for potential wind turbine sites near a forest canopy, therefore, leads to increased hub heights in order to avoid turbulence and

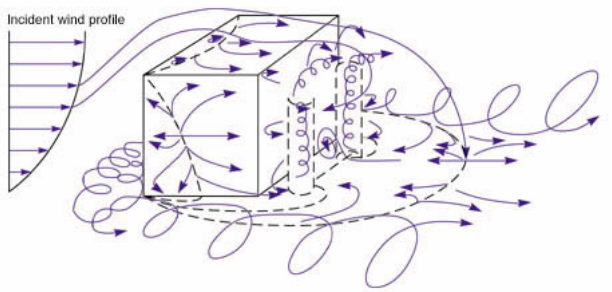

Figure 18: Conceptual representation of the flow around a building (*Simulating How the Wind Blows, Lawrence Livermore National Laboratory*, n.d.)

vertical wind shear effects. While modeling such wind conditions in urban areas, forested areas need to be modeled carefully so that their effects are taken into account. One way is to model the forests as a porous medium through which wind is passing and reaching the urban built-up areas.

4.2 Atmospheric boundary layer simulations for Urban Canopy flows

Numerical simulations on the urban atmospheric boundary layer are primarily addressed to three important areas: wind conditions at the pedestrian level and wind resource assessment dispersion of pollutants around buildings (Blocken, 2019). Different types of tools are used, such as RANS, LES, URANS, or hybrid RANS/LES, based on the required computational accuracy and available resources. LES models are better performing as they resolve the large vortical structures in the turbulent flow field. This is especially important for mass transfer in the dispersion study of pollutants. It also helps deduce "dynamic loading" on structures. Several best practice guidelines are available for ABL simulations for choosing various simulation parameters such as boundary conditions, grid resolution, time step, and convergence criteria. Some of the main contributions were made as a part of the COST project Action 732 for 'Quality Assurance and Improvement of Microscale Meteorological Models' based on work of Franke and Baklanov (2007) and Blocken (2007).

RANS approach for urban canopy flows: The RANS approach has been used in wind engineering for siting wind turbines, identifying rough flow conditions that could damage the turbine blades, and modeling of wind turbine wakes. A detailed review of the different turbulent modeling approaches is found in (Blocken, 2019) with a brief discussion on the flow equations and boundary conditions. The turbulence model coefficients are modified when the flow deviates from a homogeneous flow. The modification is based on the work of Gorle, Beeck, Rambaud, and van Tendeloo (2009) to include a building influence area (BIA). The BIA concept was further developed by Parente, Gorlé, Beeck, and Benocci (2011) and Longo and Ferrarottia (2017) based on the deviation of local turbulence properties based on the relative difference in velocity between the local flow and undisturbed homogeneous ABL and the deviation of the location from parallel shear flow based on the definition of a marker.

LES for urban canopy flows: Immer (Christian, n.d.) focused on the understanding of local turbulence structures in urban canyons using an LES approach. Artificial turbulence was generated as an input using a filtered noise approach (Klein, Sadiki, & Janicka, 2003). The method was implemented in OpenFOAM, and the model was validated using time-resolved PIV measurements. The model was then applied to a model apartment building and was capable of producing the typical turbulence flow features such as horse-shoe vortices and corner streams around buildings.

Some models have been developed to capture the influence of rough terrains without explicitly solving it. Similar to RANS formulations, most models are based on wall functions with some appropriate modifications. As Deskos, that combines wall stress models and free slip (Deskos, Laizet, & Palacios,

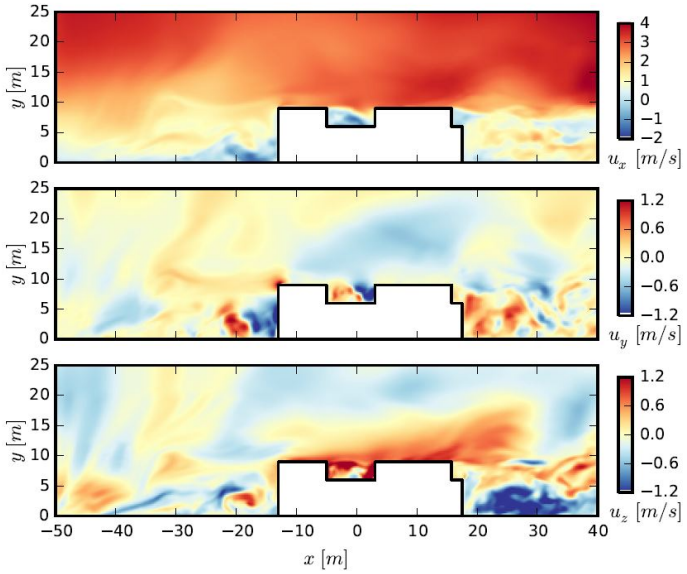

Figure 19: Instantaneous velocity profiles on a vertical plane around an isolated building. Taken from: (Christian, n.d.).

2020). The stress uses rough wall models (Chin-Hoh, 1984; Bou-Zeid, Meneveau, & Parlange, 2005), is express as:

$$\tau_{wall}(x,z) = \tau_w(x,y)\frac{\hat{\tilde{u}}_i(x,\Delta y/2,z)}{\sqrt{\hat{\tilde{u}}_x^2(x,\Delta y/2,z)+\hat{\tilde{u}}_z^2(x,\Delta y/2,z)}}, \tag{1}$$

$$\tau_w(x,z) = -\left(\frac{\kappa}{ln\left[\frac{\delta y/2}{y_0}\right]}\right)^2\left(\hat{\tilde{u}}_x^2(x,\Delta y/2,z)+\hat{\tilde{u}}_z^2(x,\Delta y/2,z)\right), \tag{2}$$

Another approach is using a classic wall model and including an extra source term for the momentum equation of the Navier–Stokes that includes the effects of the floor roughness, which can model the different types of roughness (i.e., buildings and vegetation). This source term (S_i) for buildings is modeled as blocks and can be determined as (Liu, Ishihara, He, & Niu, 2016):

$$S_i = -\frac{1}{2}\rho C_{f_i}\frac{\gamma_0}{l_0}|u|u_i \tag{3}$$

where C_{f_i} is the drag coefficient in the i direction, l_0 is the representative length and γ_0 is the physical solid packing density. These last variables are defined as:

$$l_0 = \frac{V_u}{V_{grid}}, \tag{4}$$

$$\gamma_0 = \frac{V_u}{S_u/4}, \tag{5}$$

, where V_{grid} is the computational grid volume, V_u is the computational solid volume (of the blocks), and S_u is the projective area of the solid. There have been developments of models for the drag coefficient, such as the one from Enoki (Enoki & Ishihara, 2012), obtained by fitting experimental data:

$$C_{f_i} = \frac{1}{(1-\gamma_0)^3} min\left(\frac{1.53}{1-\gamma_0}, 2.75(1-\gamma_0)\right) \tag{6}$$

For vegetation, a similar model has been proposed:

$$S_i = \frac{1}{2}\rho C_{f_i}\frac{\gamma_0}{l_0}|u|u_i \tag{7}$$

where $C_{f_i} = C_D(1-\gamma_0^2)$, C_D is a drag coefficient and has been determined experimentally.

A comprehensive of the state of the art for atmospheric boundary layer simulations is provided in the zEPHYR Deliverable 1.1 (Kale, Venkatraman, Sachar, & Elagamy, 2020).

4.3 UK power generation mix

The website "gridwatch" shows the energy mix in the UK on a daily basis. Figure 20 shows the mix on 23rd Oct 2021. Maximum energy is generated by coal and then by wind. At times, wind can generate almost 50% of the energy generated in the UK. Figure 21 shows the variation of only wind energy in the UK. It can be seen clearly that wind energy generated is very unstable. Therefore, for wind energy to become a reliable energy source is still some years away and will require a lot of effort in wind turbine and electric transmission technology.

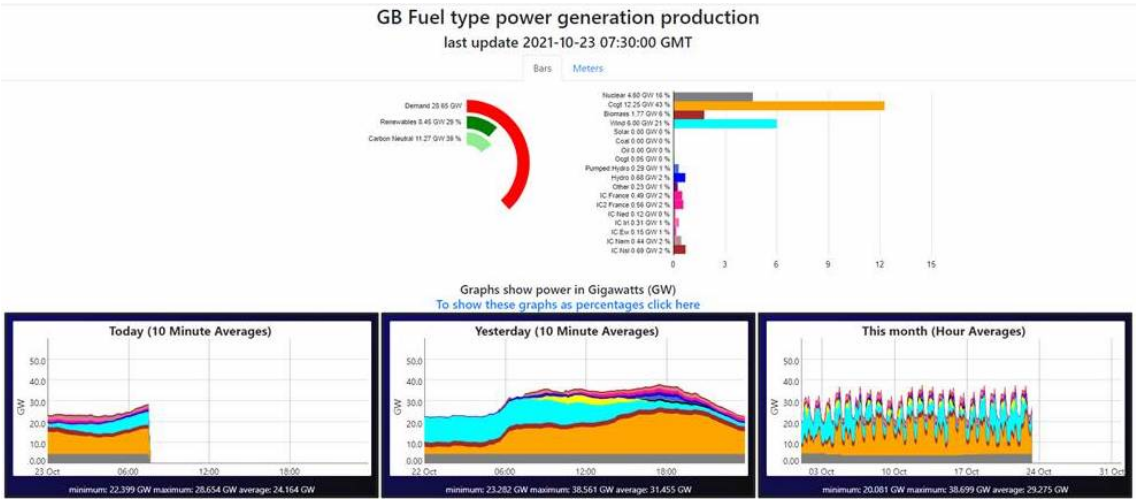

Figure 20: UK energy mix on 23rd Oct 2021

4.4 Urban environment studies for analyzing urban wind flow: A review

The urgent need to address the global climate crisis necessitates the rapid replacement of fossil fuel-based energy sources with renewable alternatives. This transition requires extensive deployment of renewable energy infrastructure. In this context, the urban environment offers several advantages in terms of facilitating distributed renewable generation. However, the insufficient understanding of wind field characteristics within urban areas has led to inadequate safety measures for Small Wind Turbines (SWT), and poor performance (Smith, Forsyth, Sinclair, & Oteri, 2012; KC, Whale, & Urmee, 2019). The wind flow patterns in built environments differ significantly from those observed over flat and open terrains (Kaimal & Finnigan, 1994), primarily due to the non-homogeneous roughness of urban areas

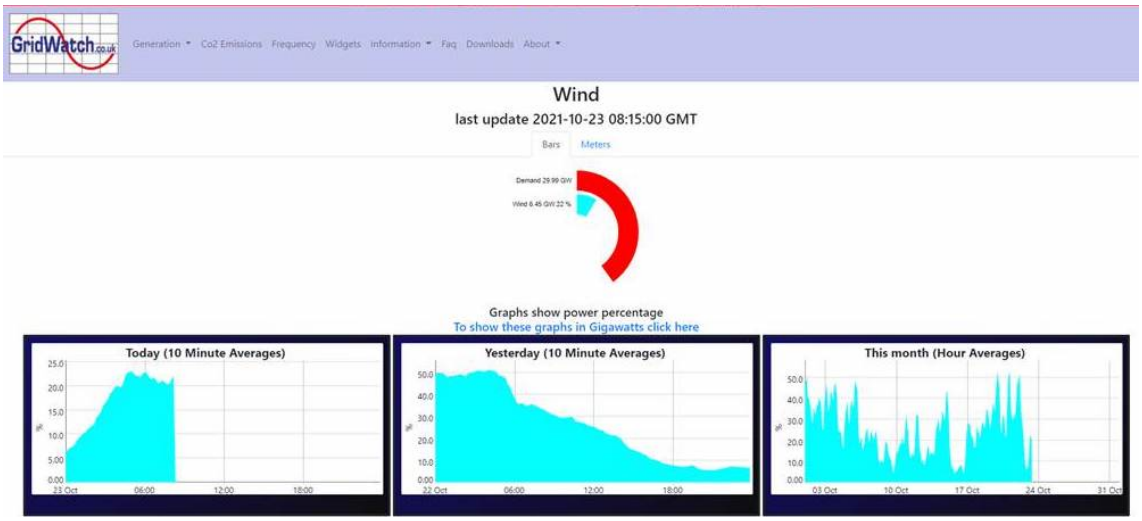

Figure 21: Variation of wind energy generated in the UK on 23rd Oct 2021

(Ricciardelli & Polimeno, 2006). Consequently, comprehending the flow characteristics in urban areas is of utmost importance to ensure structural safety and enhance the performance of SWTs (Stathopoulos et al., 2018).

Both experimental and numerical approaches contribute to understanding the characteristics of wind fields in built environments. Experimental data provided by the Architectural Institute of Japan (AIJ, 2007) and the Compilation of Experimental Data for Validation of microscale dispersion models (CEDVAL, 2006) offer insights into wind flows around individual buildings or clusters of buildings, particularly at the pedestrian level. Field measurements conducted in Oklahoma City, United States, examined wind conditions at both pedestrian and building levels, focusing on wind patterns over urban areas and their relationship to wind direction variations (Nelson et al., 2004; Nelson, Pardyjak, Klewicki, et al., 2007; Nelson, Pardyjak, Brown, & Klewicki, 2007). Turbulence spectra and cross spectra of wind velocity components were analyzed in Ł'od'z, Poland, revealing similarities between urban wind fields and those over homogeneous flat terrain described by (Kaimal et al., 1972) for the Kansas experiment. However, certain characteristics, such as peaks in the urban wind field spectra, can be attributed to phenomena specific to built environments, such as conical vortex (Nelson, Pardyjak, Klewicki, et al., 2007; ?, ?). The influence of wind direction on spectra was investigated at the rooftop of a warehouse in Port Kennedy, Western Australia (Tabrizi et al., 2015). Moreover, the presence of buildings affects the integral length scales of velocity components, as demonstrated by (Christen et al., 2007).

Numerical approaches, particularly Computational Fluid Dynamics (CFD), have also been employed to study urban airflow at building rooftops. Several studies have reviewed these approaches (Micallef & Van Bussel, 2018; Stathopoulos et al., 2018; Toja-Silva et al., 2018; KC et al., 2019). The impact of building height, urban configuration, and rooftop shape on wind flow characteristics was investigated (Abohela et al., 2013). Additionally, the influence of roof shapes on turbulence intensity and mean velocity over building roofs was examined (Toja-Silva et al., 2015). Previous investigations predominantly utilized the Reynolds-averaged Navier-Stokes (RANS) approach, which provides mean wind field statistics (Vita, 2020). However, for a more comprehensive understanding of urban wind field characteristics, including second-order statistics like spectra and covariance, and for more accurate and reliable results, high-fidelity numerical methods like Large Eddy Simulations (LES) are required (Blocken, 2015, 2018). While some studies using LES have focused on simulating wind fields over built environments to assess the dispersion of pollutants (Merlier et al., 2019) and pedestrian comfort (Tolias et al., 2018; Jacob & Sagaut, 2018), a thorough description of wind field characteristics at the rooftop, including second-order statistics, has not been presented (Kono et al., 2016).

4.5 Power production estimation of wind turbines in the city of Nottingham

4.5.1 Wind conditions in Nottingham

The city of Nottingham is centrally located on the island of Great Britain, and therefore, it experiences turbulent wind conditions coming from surrounding cities. This makes wind velocity and wind directions highly unsteady at any location within the city (and around) almost throughout the year. In the present study, Nottingham wind conditions were recorded using weather stations at two different locations named Watnall and Sutton Bonington, both at a height of 43 meters. While Watnall is located northwest of Nottingham and falls within the bigger area of the city, Sutton is located in the southwest and is far away from any urban agglomeration. Figure 22 shows the raw data of wind velocity recorded at the two locations for a period of 4 years. The data shown are averaged over a period of every 1 hour.

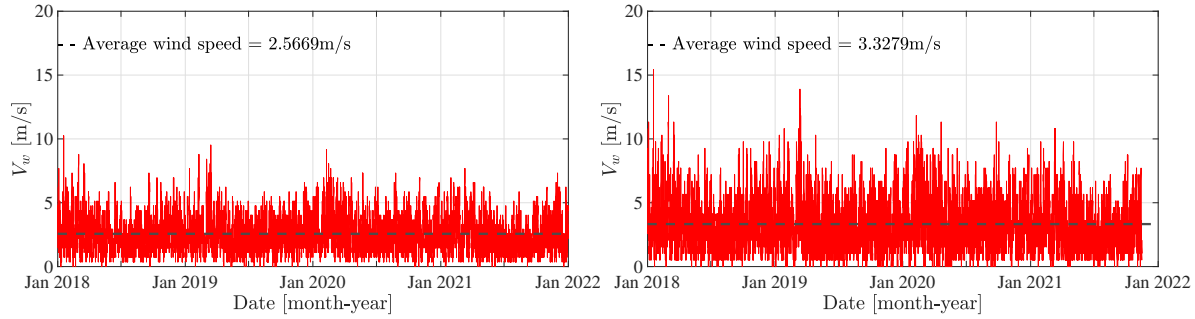

(a) Watnall **(b)** Sutton

Figure 22: Wind conditions

Both locations show highly unsteady wind conditions when seen on a yearly scale. The yearly average wind speed at Watnall is less than at Sutton. The nearby buildings around the Watnall location increase the turbulence content and decrease the wind speed which happens to a lesser extent in the case of Sutton. Therefore, if a standalone off-grid wind turbine is placed within the urban agglomeration, although it will avoid transmission losses, the wind speed encountered will be less as compared to a rural location. For further analyses, Watnall is chosen as it provides more realistic data for urban wind turbines.

4.5.2 Small-scale wind turbines

The current study assumes that wind turbines are placed at exactly the same location as the weather station at Watnall. A total of five wind turbines are selected, shown in Table 4, the power curves of which are already available in the literature. Power predicted based on Watnall wind conditions is shown in Fig. 23.

Table 4: Wind turbines selected for power performance investigation in the city of Nottingham

Wind turbine	Type	Diameter [m]	Height [m]
QR6 (Revolution, n.d.)	Darrieus - Helical	3.13	5.1
TURBY (Van Bussel, Polinder, & Sidler, 2004)	Darrieus - Helical	2	3
Battisti (Battisti et al., 2018)	Darrieus - Straight	1.028	1.46
Battisti (Battisti et al., 2018)	Darrieus - Troposkien	1.51	1.51
Doerffer (Doerffer, Doerffer, Ochrymiuk, & Telega, 2019)	Savonius - twin rotor	1.2	3.3

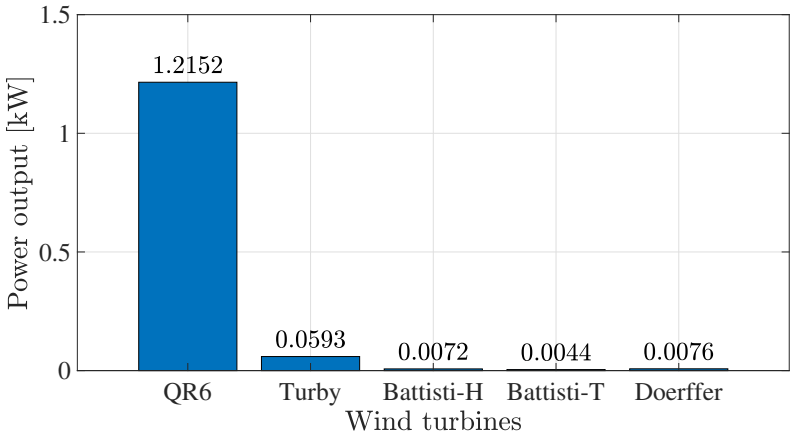

Figure 23: Wind turbines

The highest power is predicted by QR6 and has a huge difference from all the other wind turbines. Both the helical designs perform better than all of them, and the lowest power is predicted by the troposkien shape wind turbine. Based on previous experience, there are two reasons for the observed difference in power. First is the variation in size or swept area of the wind turbine, which influences the total oncoming wind power. Second is the variation in VAWT aerodynamic design which influences the fluid dynamic interactions with the blades. An important thing to note is that the reaction of the wind turbine to the sudden fluctuations in wind (gusts) is neglected. This is due to the time interval of 1 hour and it is assumed that 1 hour is enough time for the wind turbine to average out such unsteady fluctuations. In the next section, full 3D design space will be investigated by keeping a constant swept area. This will help to understand the effect of each design parameter and the best suitable choice for a city such as Nottingham.

4.6 Urban Canopy Benchmark for zEPHYR project - Clifton Campus at Nottingham Trent University

As part of the zEPHYR project, the city of Nottingham is chosen as the benchmark for the Urban Canopy. The aim is to map the whole city for the wind conditions present throughout the year. This will help to decide the best available location for setting up urban vertical axis wind turbines. For the initial phase, the two campuses of Nottingham Trent University has been chosen: City campus and Clifton campus.

Figure 24 shows a bird-eye view of the city campus. The city campus is located right at the center of Nottingham and very close to the city centre. Therefore, the locality surrounding the city campus is dense with a number of buildings close-by. The tallest building is Newton building, which is amongst the tallest in the whole of Nottingham. Although Newton building would be ideal for a rooftop wind turbine, there are Falcon birds which nests on the roof round the year. Since the birds are a protected species in the UK, it is illegal to place any rotating machines nearby the roof, thereby, removing any possibility of either a wind anemometer or a wind turbine. The second building in focus is Chaucer building. There is a weather station already installed on the rooftop and the wind conditions are being monitored every day. The weather station is placed just 2 metres above the roof level, therefore, there is a possibility that wind velocities recorded are affected by the boundary layer (or separated flow) on the roof. In the coming months, the weather station will be raised to atleast 6 metres or a separate anemometer will be installed to check the improvement in wind velocities measured.

Figure 25 shows the Clifton campus of NTU. The campus is on the outskirts of Nottingham, so it is in a much more sparsely populated or open area. Therefore, wind conditions in this campus are expected to be better suited for an urban wind turbine, as compared to the city campus. Most of the buildings within

Figure 24: NTU City Campus

the Clifton campus have fragile roofs, therefore not suited to support the strong foundation needed for a small wind turbine. Therefore, it has been decided to install the wind turbine on the ground in an open area. The exact location of the installation will depend on various factors such as availability of space for the foundation, wiring needed to connect the wind turbine to other equipment, presence of trees nearby, objections (if any) by local NTU staff, etc.

Figure 25: NTU Clifton Campus

For now, the Clifton campus is chosen for Urban Canopy benchmark studies. The major reason is the lack of adequate space on the ground in the City campus. Therefore, two major activities will be undertaken: atmospheric boundary layer simulations of the whole campus and installation of the wind turbine and measuring its performance and noise. Section 4.2 deals with the former, and section **??** deals with the latter.

4.6.1 Flow solver methodology - Lattice Boltzmann Method

The Lattice Boltzmann Method (LBM) is used to compute the flow field because it was shown to be accurate and efficient for similar low Reynolds number rotor applications (Brandetti et al., 2023) (Gourdain, Jardin, Serre, Prothin, & Moschetta, 2018). The commercial software 3DS Simulia PowerFLOW is used and has already been validated for aerodynamic and aeroacoustic studies on rotors, in general, (Avallone et al., 2019; Casalino, Hazir, & Mann, 2018; Nardari et al., 2019). The software solves the discrete Lattice Boltzmann (LB) equation for a finite number of directions. For a detailed description of the method, the reader can refer to Succi (Succi, 2001) and Shan et al. (Shan, Yuan, & Chen, 2006) while to Chen and Doolen (S. Chen & Doolen, 1998) for a review. The LB method determines the macroscopic flow variables starting from the mesoscopic kinetic equation, i.e., the LB equation. The discretization used for this particular application consists of 19 discrete velocities in three dimensions (D3Q19), involving a third-order truncation of the Chapman-Enskog expansion (H. Chen, Chen, & Matthaeus, 1992). The distribution of particles is solved by means of the LB equation on a Cartesian mesh, known as a lattice. An explicit time integration and a collision model are used. For the collision term, the formulation based on a unique Galilean invariant (H. Chen, Zhang, & Gopalakrishnan, 2015) is used. The equilibrium distribution of Maxwell-Boltzmann is adopted (H. Chen et al., 1992).

To take into account the effect of the sub-grid unresolved scales of turbulence, a Very Large Eddy Simulation (VLES) model is implemented. Following Yakhot and Orszag (Yakhot & Orszag, 1986), a two-equations $k - \epsilon$ Renormalization Group is used to compute a turbulent relaxation time that is added to the viscous relaxation time. To reduce the computational cost, a pressure-gradient-extended wall model is used to approximate the no-slip boundary condition on solid walls (Teixeira, 1998; Wilcox, 2006). The model is based on the extension of the generalized law-of-the-wall model (Launder & Spalding, 1974) to take into account the effect of the pressure gradient. These equations are iteratively solved from the first cell close to the wall in order to specify the boundary conditions of the turbulence model. For this purpose, a slip algorithm (S. Chen & Doolen, 1998), obtained as a generalization of a bounce-back and specular reflection process, is used.

Far-field noise is computed using the Ffowcs Williams and Hawkings (Ffowcs Williams & Hawkings, 1969) (FW-H) acoustic analogy. In particular, the formulation 1A of Farassat and Succi (Farassat & Succi, 1980) extended to a convective wave equation is used in this study (Brès, Pérot, & Freed, 2009). The formulation has been implemented in the time domain using a source-time dominant algorithm (Casalino, 2003). Pressure fluctuations are recorded on three permeable surfaces enclosing the wind turbine and its wake. These pressure fluctuations are used as input to the FW-H solver, thereby including all noise sources inside the three surfaces. Pressure fluctuations are also captured on all solid surfaces (blade surfaces), which, when input to the FW-H solver will include noise sources only on the solid surfaces.

4.6.2 Wind turbine geometry

The Clifton campus of Nottingham Trent University is surveyed, and a CAD geometry is prepared out of it. The CAD model combines the 2D plan of all the buildings on the campus with the height of each building measured in the survey. The Clifton campus virtual model is input as a solid geometry in the PowerFLOW setup. The geometry and setup are shown in Figure 26 and 27. The inclusion of all the buildings is expected to result in stronger three-dimensional (3D) effects and increased fluid dynamic interactions with other buildings. These fluid dynamic interactions are expected to lead to differences in the unsteadiness of loading on each building, which, in turn, affects the wake dynamics and behavior of any wind turbine in the vicinity.

The current study involves the high-fidelity Lattice Boltzmann Method (LBM) to simulate the Clifton campus setup with the freestream velocity of 4 m/s. Various upstream structures have been used to mimic freestream turbulence prevalent in an urban boundary layer.

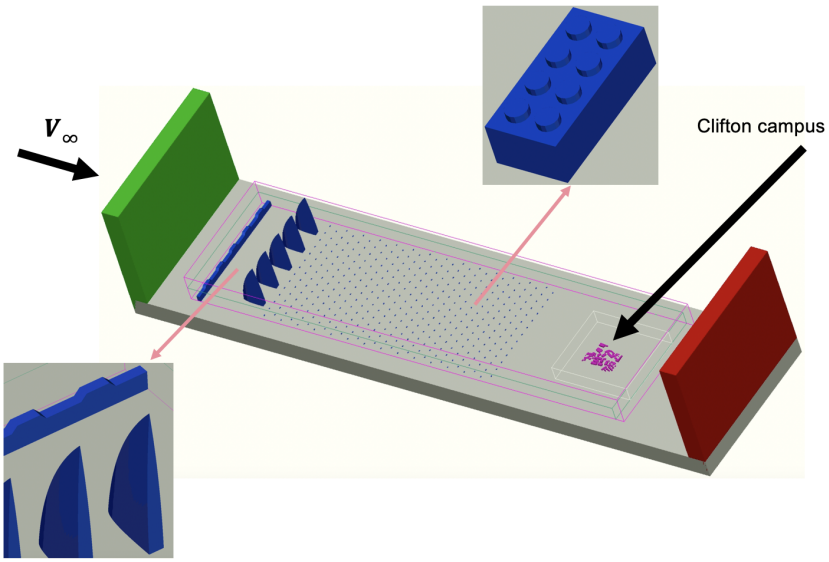

(a)

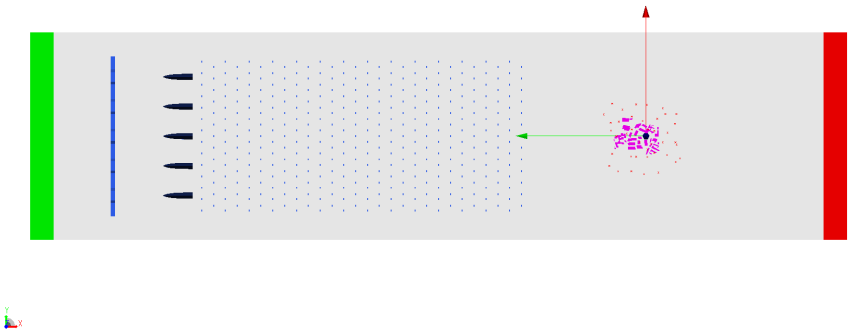

(b)

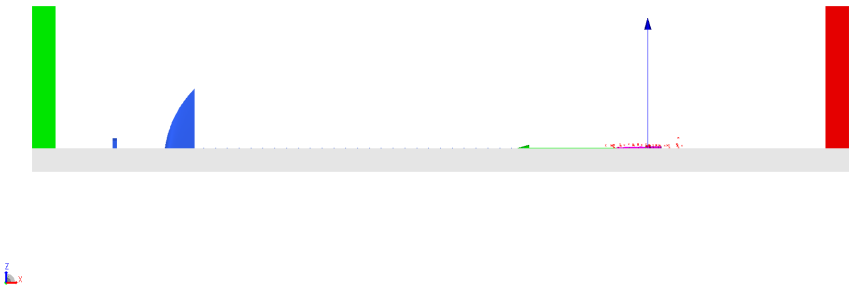

(c)

Figure 26: PowerFLOW numerical setup

4.6.3 Numerical setup

A simulation volume is implemented as shown in Figure 26. The velocity inlet is set to the freestream velocity V_∞. An ambient pressure of 101.325 kPa is applied at the pressure outlet. The building surfaces

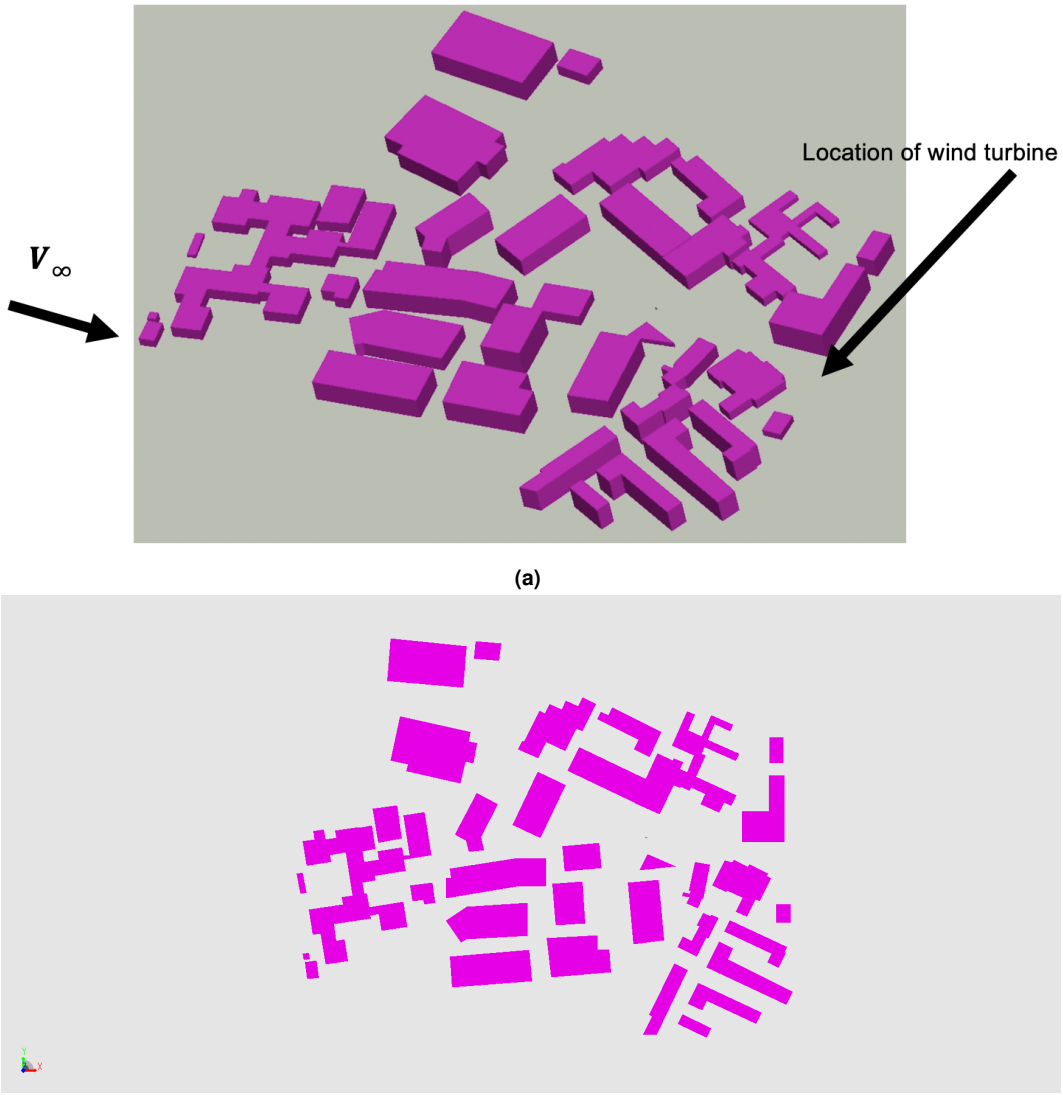

Figure 27: Clifton campus geometry

are subjected to a no-slip boundary condition. PowerFLOW generates a Cartesian volume grid around the individual solid components in the domain by beginning with the minimum hexahedral cell (voxel) size and a specified number of variable resolution (VR) levels. The VR levels are arranged in a range from fine to coarse, with a voxel size change factor of 2 between adjacent VRs, which creates distinct VR regions. The software automatically intersects the Cartesian mesh with the solid parts to produce a collection of polygons, or surfels, that represent the true surface of the body. To optimize computational efficiency, the present study utilizes 4 VR regions, with higher resolutions near the buildings and coarser regions located farther away. This methodology permits the allocation of computational effort primarily to areas of interest and where high-flow gradients are anticipated. The current computational setup has been partially adopted from previous works by Shubham et al. (Shubham, Wright, & Ianakiev, 2022; Shubham, Wright, Avallone, & Ianakiev, 2023).

The freestream velocity is kept constant at 4 m/s, which corresponds to the average wind speed in the city of Nottingham, measured over 4 years. The values of freestream turbulence intensity (I_t) and turbulence length scale (L_t) are set to 0.1% and 1 mm, respectively. However, it is anticipated that

the upstream structures used in the setup will introduce significant turbulent content to represent actual urban wind conditions. The simulations are conducted using a Linux workstation equipped with an AMD Ryzen Threadripper 3990X Gen3 64 Core 128GB DDR4 3GHz platform.

4.6.4 Results

The velocity contour results can be seen in Figures 28 and 29. As expected, the upstream structures increased the turbulence content significantly before it approached the Clifton campus model. The freestream velocity experienced by the campus is less than 4 m/s and is highly turbulent. In Figure 28 (b), the formation of an urban canopy/urban boundary layer can be seen over the buildings on the Clifton campus. The average height of the building is 6 m. The wind turbine, which is planned to be installed on the campus (shown by the black arrow in the figure), is 15 m in height. Figure 29 (b) shows the variation in instantaneous freestream velocity with height at the location of installation of the wind turbine. The black dotted line shows the height of the wind turbine (15 m). The velocity that the wind turbine is predicted to experience is 2.4 m/s, which is above the cut-in wind speed of the QR6 wind turbine (2 m/s), which will be installed.

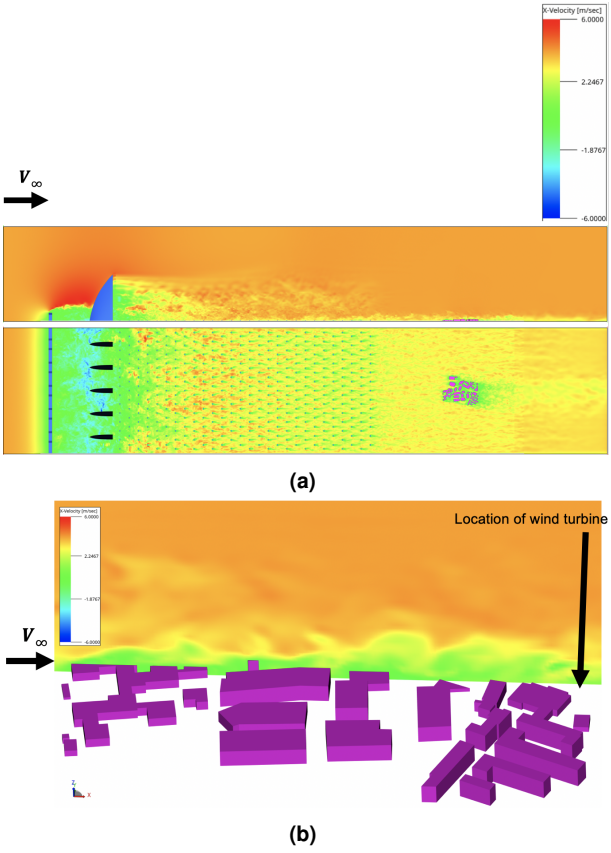

Figure 28: Velocity contour results

Figure 29 (a) shows an increased velocity region just upstream of the location of the wind turbine. This is due to the "funnel effect" created by the upstream buildings and is beneficial for the wind turbine in terms of increasing the power generation values.

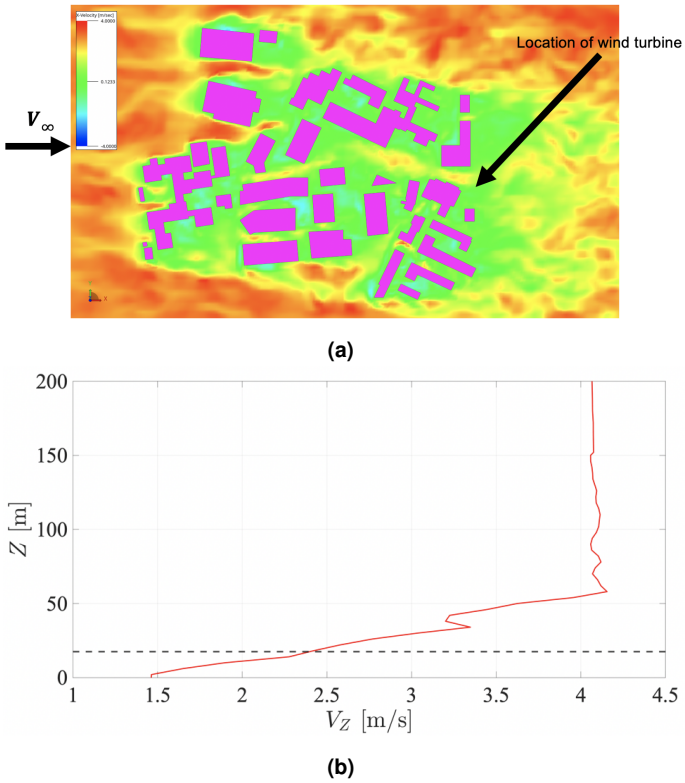

Figure 29: Velocity contour results

5 Conclusions

This report presented a summary of the work conducted on the three benchmarks of the project zEPHYR within the work package # 5. The main objectives of the project were achieved. Public databases were published to share the available literature.

Acknowledgments

This project has received funding from the European Union's Horizon 2020 research and innovation program under grant agreement No EC grant 860101. We are grateful to that and the members who are not listed as co-authors for their helpful discussions and comments.

References

Abohela, I., Hamza, N., & Dudek, S. (2013). Effect of roof shape, wind direction, building height and urban configuration on the energy yield and positioning of roof mounted wind turbines. *Renewable Energy*, *50*, 1106–1118. Retrieved from https://www.sciencedirect.com/science/article/pii/S0960148112005381 doi: https://doi.org/10.1016/j.renene.2012.08.068

AIJ. (2007). *Architectural institute of Japan, guidebook for CFD predictions of urban wind environment.* Retrieved from https://www.aij.or.jp/jpn/publish/cfdguide/index_e.htm

Avallone, F., van den Ende, L., Li, Q., Ragni, D., Casalino, D., Eitelberg, G., & Veldhuis, L. (2019). Aerodynamic and aeroacoustic effects of swirl recovery vanes length. *Journal of Aircraft*, *56*(6), 2223–2235.

Battisti, L., Persico, G., Dossena, V., Paradiso, B., Castelli, M. R., Brighenti, A., & Benini, E. (2018). Experimental benchmark data for h-shaped and troposkien vawt architectures. *Renewable energy*, *125*, 425–444.

Blocken, B. (2015). Computational Fluid Dynamics for urban physics: Importance, scales, possibilities, limitations and ten tips and tricks towards accurate and reliable simulations. *Building and Environment*, *91*, 219-245. Retrieved from https://www.sciencedirect.com/science/article/pii/S0360132315000724 doi: https://doi.org/10.1016/j.buildenv.2015.02.015

Blocken, B. (2018). LES over RANS in building simulation for outdoor and indoor applications: A foregone conclusion? *Building Simulation*, *11*(4), 821–870. doi: 10.1007/s12273-018-0459-3

Blocken, B. (2019). *Introduction to the simulation of atmospheric flows* (Vol. 1). Belgium: von Karman Institute for Fluid Dynamics.

Bou-Zeid, E., Meneveau, C., & Parlange, M. (2005, feb). A scale-dependent lagrangian dynamic model for large eddy simulation of complex turbulent flows. *Physics of Fluids*, *17*(2), 025105. doi: 10.1063/1.1839152

Brandetti, L., Avallone, F., De Tavernier, D., LeBlanc, B., Ferreira, C. S., & Casalino, D. (2023). Assessment through high-fidelity simulations of a low-fidelity noise prediction tool for a vertical-axis wind turbine. *Journal of Sound and Vibration*, *547*, 117486.

Brès, G., Pérot, F., & Freed, D. (2009). Properties of the lattice boltzmann method for acoustics. In *15th aiaa/ceas aeroacoustics conference (30th aiaa aeroacoustics conference)* (p. 3395).

Buhl, M. L. (2011). *Wt_perf, nwtc design code.* http://wind.nrel.gov/designcodes/simulators/wtperf/.

Casalino, D. (2003). An advanced time approach for acoustic analogy predictions. *Journal of Sound and Vibration*, *261*(4), 583–612.

Casalino, D., Hazir, A., & Mann, A. (2018). Turbofan broadband noise prediction using the lattice boltzmann method. *AIAA Journal*, *56*(2), 609–628.

CEDVAL. (2006). *Compilation of Experimental Data for Validation of Microscale Dispersion Models.* Hamburg, Germany.

Chen, H., Chen, S., & Matthaeus, W. (1992, 4). Recovery of the Navier-Stokes equations using a lattice-gas Boltzmann method. *Physical Review A*, *45*(8), R5339-R5342. Retrieved from https://link.aps.org/doi/10.1103/PhysRevA.45.R5339 doi: 10.1103/PhysRevA.45.R5339

Chen, H., Zhang, R., & Gopalakrishnan, P. (2015, 8). *Lattice Boltzmann Collision Operators Enforcing Isotropy and Galilean Invariance.* Retrieved from https://patents.google.com/patent/US20150356217A1/en

Chen, S., & Doolen, G. (1998, 1). Lattice Boltzmann method for fluid flows. *Annual Review of Fluid Mechanics*, *30*(1), 329–364. Retrieved from http://www.annualreviews.org/doi/10.1146/annurev.fluid.30.1.329 doi: 10.1146/annurev.fluid.30.1.329

Chin-Hoh, M. (1984, feb). A large-eddy-simulation model for the study of planetary boundary-layer turbulence. *Journal of the Atmospheric Sciences*, *41*(13), 2052–2062.

Christen, A., van Gorsel, E., & Vogt, R. (2007). Coherent structures in urban roughness sublayer turbulence. *International Journal of Climatology*, *27*(14), 1955–1968. Retrieved from https://rmets.onlinelibrary.wiley.com/doi/abs/10.1002/joc.1625 doi: https://doi.org/10.1002/joc.1625

Christian, I. M. (n.d.). *Time-resolved measurement and simulation of local scale turbulent urban flow* (Unpublished doctoral dissertation). ETH Zurich.

Christophe, B. S. S. C., Julien, & Oerlemans, S. (2022). *zephyr - large on shore wind turbine benchmark (1.0) [data set].* doi: 10.5281/zenodo.7323750

Churchfield, M. (2013). A method for designing generic wind turbine models representative of real turbines and generic siemens swt-2.3-93 and vestas v80 specifications. *National Renewable Energy Laboratory, Golden, Colorado*.

Deskos, G., Laizet, S., & Palacios, R. (2020, jan). WInc3d: A novel framework for turbulence-resolving simulations of wind farm wake interactions. *Wind Energy*, *23*(3), 779–794. doi: 10.1002/we.2458

Doerffer, P., Doerffer, K., Ochrymiuk, T., & Telega, J. (2019). Variable size twin-rotor wind turbine. *Energies*, *12*(13), 2543.

DTU. (2021). *Technical university of denmark online meteorological data.* `http://rodeo.dtu.dk/rodeo/`.

Enoki, K., & Ishihara, T. (2012). A generalized canopy model and its application to the prediction of urban wind climate. *Journal of Japan Society of Civil Engineers, Ser. A1 (Structural Engineering & Earthquake Engineering (SE/EE))*, *68*(1), 28–47. doi: 10.2208/jscejseee.68.28

Farassat, F., & Succi, G. P. (1980). A review of propeller discrete frequency noise prediction technology with emphasis on two current methods for time domain calculations. *Journal of Sound and Vibration*, *71*(3), 399–419.

Ffowcs Williams, J. E., & Hawkings, D. L. (1969). Sound generation by turbulence and surfaces in arbitrary motion. *Philosophical Transactions of the Royal Society of London. Series A, Mathematical and Physical Sciences*, *264*(1151), 321–342.

Franke, J., & Baklanov, A. (2007). *Best practice guideline for the cfd simulation of flows in the urban environment: Cost action 732 quality assurance and improvement of microscale meteorological models*.

Gorle, C., Beeck, J., Rambaud, P., & van Tendeloo, G. (2009, 01). Cfd modelling of small particle dispersion: The influence of the turbulence kinetic energy in the atmospheric boundary layer. *Atmospheric Environment*, *43*, 673-681. doi: 10.1016/j.atmosenv.2008.09.060

Gourdain, N., Jardin, T., Serre, R., Prothin, S., & Moschetta, J.-M. (2018). Application of a lattice boltzmann method to some challenges related to micro-air vehicles. *International Journal of Micro Air Vehicles*, *10*(3), 285–299.

Jacob, J., & Sagaut, P. (2018). Wind comfort assessment by means of large eddy simulation with lattice Boltzmann method in full scale city area. *Building and Environment*, *139*, 110-124. Retrieved from `https://www.sciencedirect.com/science/article/pii/S0360132318302750` doi: https://doi.org/10.1016/j.buildenv.2018.05.015

Kaimal, J. C., & Finnigan, J. J. (1994). *Atmospheric boundary layer flows: their structure and measurement*.

Kaimal, J. C., Wyngaard, J., Izumi, Y., & Coté, O. (1972). Spectral characteristics of surface-layer turbulence. *Quarterly Journal of the Royal Meteorological Society*, *98*(417), 563–589.

Kale, B., Venkatraman, K., Sachar, S., & Elagamy, M. (2020). *Abl simulation technologies: State-of-the-art* (Tech. Rep.). zEPHYR Project Deliverable 1.1.

KC, A., Whale, J., & Urmee, T. (2019). Urban wind conditions and small wind turbines in the built environment: A review. *Renewable Energy*, *131*, 268-283. Retrieved from `https://www.sciencedirect.com/science/article/pii/S0960148118308474` doi: https://doi.org/10.1016/j.renene.2018.07.050

Klein, M., Sadiki, A., & Janicka, J. (2003, 04). A digital filter based generation of inflow data for spatially developing direct numerical or large eddy simulation. *Journal of Computational Physics*, *186*, 652-665. doi: 10.1016/S0021-9991(03)00090-1

Kono, T., Kogaki, T., & Kiwata, T. (2016). Numerical Investigation of Wind Conditions for Roof-Mounted Wind Turbines: Effects of Wind Direction and Horizontal Aspect Ratio of a High-Rise Cuboid Building. *Energies*, *9*(11), 907. doi: 10.3390/en9110907

Launder, B., & Spalding, D. (1974, 3). The numerical computation of turbulent flows. *Computer Methods in Applied Mechanics and Engineering*, *3*(2), 269–289. Retrieved from http://www.sciencedirect.com/science/article/pii/0045782574900292 doi: 10.1016/0045-7825(74)90029-2

Leloudas, G. (2006). *Optimization of wind turbineswith respect to noise* (master's thesis). Technical University of Denmark, Technical University of Denmark, Anker Engelunds Vej 1, Building 101A, 2800 Kgs. Lyngby.

Liu, Z., Ishihara, T., He, X., & Niu, H. (2016, aug). LES study on the turbulent flow fields over complex terrain covered by vegetation canopy. *Journal of Wind Engineering and Industrial Aerodynamics*, *155*, 60–73. doi: 10.1016/j.jweia.2016.05.002

Longo, R., & Ferrarottia, M. (2017, 05). Advanced turbulence models and boundary 2 conditions for flows around different configurations of 3 ground-mounted buildings. *Journal of Wind Engineering and Industrial Aerodynamics*, *167*, 160-182. doi: https://doi.org/10.1016/j.jweia.2017.04.015

Meier, P. H. (2012). *Can wind farms and forests mix?*

Merlier, L., Jacob, J., & Sagaut, P. (2019). Lattice-Boltzmann large-eddy simulation of pollutant dispersion in complex urban environment with dense gas effect: Model evaluation and flow analysis. *Building and Environment*, *148*, 634-652. Retrieved from https://www.sciencedirect.com/science/article/pii/S0360132318307042 doi: https://doi.org/10.1016/j.buildenv.2018.11.009

Micallef, D., & Van Bussel, G. (2018). A Review of Urban Wind Energy Research: Aerodynamics and Other Challenges. *Energies*, *11*(9). Retrieved from https://www.mdpi.com/1996-1073/11/9/2204 doi: 10.3390/en11092204

Micallef, D., & van Bussel, G. (2018, 08). A review of urban wind energy research: Aerodynamics and other challenges. *Energies*, *11*, 2204. doi: 10.3390/en11092204

Nardari, C., Casalino, D., Polidoro, F., Coralic, V., Lew, P.-T., & Brodie, J. (2019). Numerical and experimental investigation of flow confinement effects on uav rotor noise. In *25th aiaa/ceas aeroacoustics conference* (p. 2497).

Negre, F. (2020). The european union and forests. *Fact Sheets on the European Union - 2020*.

Nelson, M. A., Brown, M. J., Pardyjak, E. R., & Klewicki, J. C. (2004, August). Turbulence within and above real and artificial urban canopies. In *AMS 5th Symposium on the Urban Environment.* Retrieved from https://www.osti.gov/biblio/977786

Nelson, M. A., Pardyjak, E. R., Brown, M. J., & Klewicki, J. C. (2007). Properties of the wind field within the Oklahoma City Park Avenue street canyon. Part II: Spectra, cospectra, and quadrant analyses. *Journal of Applied Meteorology and Climatology*, *46*(12), 2055 - 2073. doi: https://doi.org/10.1175/2006JAMC1290.1

Nelson, M. A., Pardyjak, E. R., Klewicki, J. C., Pol, S. U., & Brown, M. J. (2007). Properties of the wind field within the Oklahoma City Park Avenue street canyon. Part I: Mean flow and turbulence statistics. *Journal of Applied Meteorology and Climatology*, *46*(12), 2038 - 2054. Retrieved from https://journals.ametsoc.org/view/journals/apme/46/12/2006jamc1427.1.xml doi: https://doi.org/10.1175/2006JAMC1427.1

Ng, E., YUAN, C., Chen, L., Ren, C., & Fung, J. (2011, 05). Improving the wind environment in high-density cities by understanding urban morphology and surface roughness: A study in hong kong. *Landscape and Urban Planning*, *101*, 59-74. doi: 10.1016/j.landurbplan.2011.01.004

Parente, A., Gorlé, C., Beeck, J., & Benocci, C. (2011, 09). A comprehensive modelling approach for the neutral atmospheric boundary layer: Consistent inflow conditions, wall function and turbulence model. *Boundary-Layer Meteorology*, *140*, 411-428. doi: 10.1007/s10546-011-9621-5

Perdigao field experiment. (2017). https://perdigao.fe.up.pt/. (Accessed: 12 October 2021)

Revolution, Q. (n.d.). https://www.quietrevolution.com/products/.

Ricciardelli, F., & Polimeno, S. (2006). Some characteristics of the wind flow in the lower Urban Boundary Layer. *Journal of Wind Engineering and Industrial Aerodynamics*, *94*(11), 815–832. Retrieved from https://www.sciencedirect.com/science/article/pii/S0167610506000894 doi: https://doi.org/10.1016/j.jweia.2006.06.003

Shan, X., Yuan, X.-F., & Chen, H. (2006). Kinetic theory representation of hydrodynamics: a way beyond the Navier–Stokes equation. *Journal of Fluid Mechanics*, *550*, 413–441. Retrieved from http://www.journals.cambridge.org/abstract_S0022112005008153 doi: 10.1017/S0022112005008153

Shubham, S., Wright, N., Avallone, F., & Ianakiev, A. (2023). Aerodynamic and aeroacoustic investigation of vertical axis wind turbines with different number of blades using mid-fidelity and high-fidelity methods. In *Aiaa aviation 2023 forum* (p. 3642).

Shubham, S., Wright, N., & Ianakiev, A. (2022). Application of richardson extrapolation method to aerodynamic and aeroacoustic characteristics of low reynolds number vertical axis wind turbines. In *28th aiaa/ceas aeroacoustics 2022 conference* (p. 3022).

Simulating how the wind blows, lawrence livermore national laboratory. (n.d.). https://str.llnl.gov/str/October01/Lee.html. (Accessed: 21 August 2020)

Smith, J., Forsyth, T., Sinclair, K., & Oteri, F. (2012). *Built-environment wind turbine roadmap* (Tech. Rep.). National Renewable Energy Lab.(NREL), Golden, CO (United States). Retrieved from https://www.nrel.gov/docs/fy13osti/50499.pdf

Stathopoulos, T., Alrawashdeh, H., Al-Quraan, A., Blocken, B., Dilimulati, A., Paraschivoiu, M., & Pilay, P. (2018). Urban wind energy: Some views on potential and challenges. *Journal of Wind Engineering and Industrial Aerodynamics*, *179*, 146-157. Retrieved from https://www.sciencedirect.com/science/article/pii/S0167610517304774 doi: https://doi.org/10.1016/j.jweia.2018.05.018

Succi, S. (2001). *The lattice Boltzmann equation for fluid dynamics and beyond* (1st editio ed.). Oxford: Clarendon Press.

Tabrizi, A. B., Whale, J., Lyons, T., & Urmee, T. (2015). Extent to which international wind turbine design standard, IEC 61400-2 is valid for a rooftop wind installation. *Journal of Wind Engineering and Industrial Aerodynamics*, *139*, 50–61. Retrieved from https://www.sciencedirect.com/science/article/pii/S016761051500015X doi: https://doi.org/10.1016/j.jweia.2015.01.006

Teixeira, C. (1998, 12). Incorporating Turbulence Models into the Lattice-Boltzmann Method. *International Journal of Modern Physics C*, *09*(08), 1159–1175. Retrieved from http://www.worldscientific.com/doi/abs/10.1142/S0129183198001060 doi: 10.1142/S0129183198001060

Toja-Silva, F., Kono, T., Peralta, C., Lopez-Garcia, O., & Chen, J. (2018). A review of computational fluid dynamics (CFD) simulations of the wind flow around buildings for urban wind energy exploitation. *Journal of Wind Engineering and Industrial Aerodynamics*, *180*, 66-87. Retrieved from https://www.sciencedirect.com/science/article/pii/S0167610518302277 doi: https://doi.org/10.1016/j.jweia.2018.07.010

Toja-Silva, F., Peralta, C., Lopez-Garcia, O., Navarro, J., & Cruz, I. (2015). On roof geometry for

urban wind energy exploitation in high-rise buildings. *computation*, *3*(2), 299–325. Retrieved from https://www.mdpi.com/2079-3197/3/2/299 doi: 10.3390/computation3020299

Tolias, I., Koutsourakis, N., Hertwig, D., Efthimiou, G., Venetsanos, A., & Bartzis, J. (2018). Large Eddy Simulation study on the structure of turbulent flow in a complex city. *Journal of Wind Engineering and Industrial Aerodynamics*, *177*, 101-116. Retrieved from https://www.sciencedirect.com/science/article/pii/S0167610517309765 doi: https://doi.org/10.1016/j.jweia.2018.03.017

Van Bussel, G., Polinder, H., & Sidler, H. (2004). The development of turby, a small vawt for the built environment. In *The global windpower 2004 conference & exhibition* (pp. 1–10).

Venkatraman, K., Hågbo, T.-O., Buckingham, S., & Giljarhus, K. E. T. (2023, January). Effect of different source terms and inflow direction in atmospheric boundary modeling over the complex terrain site of perdigão. *Wind Energy Science*, *8*(1), 85–108. Retrieved from https://doi.org/10.5194/wes-8-85-2023 doi: 10.5194/wes-8-85-2023

Vita, G. (2020). *The effect of turbulence in the built environment on wind turbine aerodynamics (doctoral thesis)* (Unpublished doctoral dissertation). University of Birmingham.

Wilcox, D. (2006). *Turbulence modelling for CFD (Third Edition)*. DCW Industries, Incorporated.

Yakhot, V., & Orszag, S. (1986). Renormalization group analysis of turbulence. I. Basic theory. *Journal of Scientific Computing*, *1*(1), 3–51. Retrieved from http://link.springer.com/10.1007/BF01061452 doi: 10.1007/BF01061452